

RNA catalyses nuclear pre-mRNA splicing

Sebastian M. Fica^{1,2*}, Nicole Tuttle^{3*}, Thaddeus Novak⁴, Nan-Sheng Li⁴, Jun Lu³, Prakash Koodathingal², Qing Dai³, Jonathan P. Staley² & Joseph A. Piccirilli^{3,4}

In nuclear pre-messenger RNA splicing, introns are excised by the spliceosome, a dynamic machine composed of both proteins and small nuclear RNAs (snRNAs). Over thirty years ago, after the discovery of self-splicing group II intron RNAs, the snRNAs were proposed to catalyse splicing. However, no definitive evidence for a role of either RNA or protein in catalysis by the spliceosome has been reported so far. By using metal rescue strategies in spliceosomes from budding yeast, here we show that the U6 snRNA catalyses both of the two splicing reactions by positioning divalent metals that stabilize the leaving groups during each reaction. Notably, all of the U6 catalytic metal ligands we identified correspond to the ligands observed to position catalytic, divalent metals in crystal structures of a group II intron RNA. These findings indicate that group II introns and the spliceosome share common catalytic mechanisms and probably common evolutionary origins. Our results demonstrate that RNA mediates catalysis within the spliceosome.

Nuclear pre-mRNA splicing (Fig. 1a) is a crucial determinant of the export, translation, stability and diversity of eukaryotic messages¹, but the spliceosome is the only major cellular machinery² required for gene expression for which the catalytic components remain undefined. Nevertheless, for three decades, there has been widespread speculation that nuclear pre-mRNA splicing is catalysed by RNA.

This speculation arose from the discovery of self-splicing RNAs, the identification of snRNA components of the spliceosome, and the finding that pre-mRNA introns and group II introns both splice through an intermediate having a lariat structure^{3,4} (Fig. 1a). Since then, genetic, biochemical and NMR data have shown that the snRNAs share functional and structural similarity with the catalytic core of group II introns^{5–10}. Similarly to the catalytic domain V of group II introns, U2/U6 helix Ib and the intramolecular stem-loop (ISL) of U6 adopt a secondary structure having a conserved bulge and AGC triad sensitive to phosphorothioate substitutions and important for both steps of splicing^{5–8,10–16} (Fig. 1b, c). Extending the parallel, a recent crystal structure of a central splicing factor, Prp8, revealed domains similar to those found in cofactors of group II introns¹⁷.

Consistent with a catalytic role for RNA in the spliceosome, in the absence of spliceosomal proteins, U2 and U6 can base-pair and fold *in vitro* into a structure that catalyses reactions similar to the two steps of pre-mRNA splicing^{18,19}, although the relevance of such protein-free, minimal model systems for understanding spliceosomal catalysis has been questioned (ref. 20 and compare with ref. 21).

Whether or not through RNA, the catalytic centre of the spliceosome, like that of group II introns, was proposed to catalyse the two phosphotransesterifications of splicing by positioning two catalytic metals²². In this two-metal mechanism²², one metal would stabilize the nucleophile and the second metal would stabilize the leaving group (Fig. 1a). Indeed, in human spliceosomes, as well as group II introns²³, divalent metals stabilize the leaving group during each step of splicing^{24,25}.

Intriguingly, recent crystal structures of a group II intron have revealed that domain V utilizes five non-bridging phosphate oxygens to coordinate two metals 3.9 Å apart^{26,27}—ideally positioned to effect catalysis by the two-metal mechanism²². By analogy, the snRNAs have

been suggested to similarly position metals, consistent with early phosphorothioate substitution studies in U6 (refs 12, 13). However, only residue U80, situated in the U6 ISL, has been shown to interact with a metal^{14,28} and it has remained unclear whether U80 positions a structural or a catalytic metal. Thus, despite work highlighting similarities between self-splicing RNA and the snRNAs, there is still no direct evidence that the snRNAs mediate splicing catalysis.

Definitive evidence for a direct role for metals coordinated by the RNA in the catalysis of self-splicing group I introns has come from metal rescue strategies^{29–31}. These approaches, validated by subsequent structural studies^{31,32}, enabled the direct linkage of metal ligands in the ribozyme to the splice sites. Application of such strategies in an investigation of pre-mRNA splicing has been hindered by proofreading and discard mechanisms that compete with catalysis during both steps of splicing^{28,33–35}. Here by disabling such proofreading, we implemented metal rescue strategies in the fully assembled spliceosome and identified the direct effectors of splicing catalysis. Our results provide definitive evidence that snRNAs interact with the splice sites directly through catalytic metals during both chemical steps of splicing, establishing that the spliceosome utilizes RNA to catalyse splicing.

U6 binds metals during both splicing steps

To identify components that mediate metal catalysis in the spliceosome, we used metal rescue approaches³¹ (Fig. 2a) to find metal ligands that function at the catalytic stage and subsequently test these ligands for a direct role in positioning catalytic metals (Fig. 1a). The similarities between U6 and the catalytic domain V of group II introns suggest U6 as the best candidate for providing metal ligands that function at the catalytic stage (Fig. 1b, c). Indeed, early sulphur substitution studies implicated eight oxygens in the phosphodiester backbone of U6 as important for splicing^{12,13} (Fig. 1b). Although informative, these studies assayed sulphur substitutions only at the *pro-R_p* phosphate oxygen (phosphorothioate substitutions referred to as PS(*R_p*), Fig. 2a) and subsequent studies have only revealed rescue by thiophilic metals for U80-PS(*S_p*)^{14,28}.

To identify metal ligands, we assayed splicing in *Saccharomyces cerevisiae* extracts reconstituted with U6 bearing individual sulphur

¹Graduate Program in Cell and Molecular Biology, The University of Chicago, Chicago, Illinois 60637, USA. ²Department of Molecular Genetics and Cell Biology, Cummings Life Sciences Center, 920 East 58th Street, The University of Chicago, Chicago, Illinois 60637, USA. ³Department of Chemistry, 929 East 57th Street, The University of Chicago, Chicago, Illinois 60637, USA. ⁴Department of Biochemistry and Molecular Biology, Gordon Center for Integrative Science, 929 East 57th Street, The University of Chicago, Chicago, Illinois 60637, USA.

*These authors contributed equally to this work.

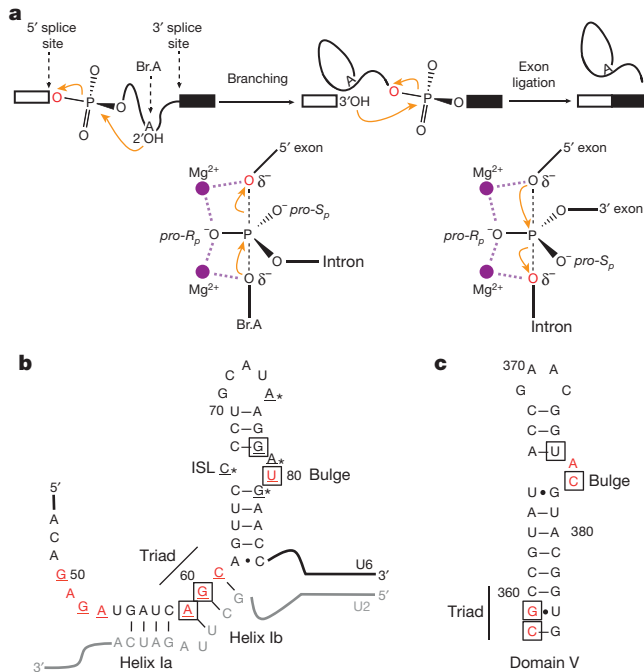


Figure 1 | Chemistry of pre-mRNA splicing and U2/U6 model showing sites sensitive to sulphur substitutions and rescued by thiophilic metal. **a**, Reaction scheme (top) and transition state diagrams (bottom) for the two steps of nuclear pre-mRNA splicing. **b**, **c**, Models of the U2/U6 structure from the spliceosome (**b**) and domain V of a group II intron (**c**). Nucleotides where sulphur substitutions were shown previously to interfere with splicing^{12–16} are coloured red; underlined U6 nucleotides were tested in this study. An asterisk indicates those positions where only the *pro-S_p* oxygen was substituted with sulphur; boxed nucleotides were found to provide ligands for metals at the catalytic stage (Fig. 2, ref. 26).

substitutions covering both the *R_p* and *S_p* diastereomers at twenty positions, on the basis of previous studies on pre-mRNA and group II splicing^{12–16,26} (Fig. 1b, c). To focus on ligand–metal interactions important during catalysis, we restricted our analysis to spliceosomes that had already undergone catalytic activation³⁶ by affinity-purifying spliceosomes using tagged Prp19p (Extended Data Fig. 1a–c). We then assayed for rescue in the absence of ATP and soluble factors, thus ensuring that spliceosomes had progressed beyond the final ATP-dependent activation step, while at the same time eliminating ATP-dependent proof-reading mechanisms^{28,34} to enhance the potential for rescue (Extended Data Fig. 1d, Supplementary Note 1).

Five of the twenty tested substitutions conferred strong branching defects (Fig. 1b). In addition to the sulphur substitutions G60-PS(*R_p*), U80-PS(*S_p*), and U80-PS(*R_p*) (Fig. 2b, h compared with 2d, f, g; first lanes) (refs 12–14), the substitutions G78-PS(*S_p*) and A59-PS(*S_p*) also caused branching defects in extract in Mg²⁺ (Fig. 2c, e, first lanes; Extended Data Fig. 2a).

In addition to spliceosomes containing U80-PS(*S_p*) (Fig. 2g; refs 14, 28), affinity-purified spliceosomes containing any of the other four sulphur substitutions that conferred a branching defect could catalyse branching in Cd²⁺ much more efficiently than in Mg²⁺ (Fig. 2c–f). Thus, all five oxygens sensitive to sulphur substitution bind metals important for branching at the catalytic stage.

To test whether these non-bridging oxygens implicated in branching also function in exon ligation, we assembled each of the twenty sulphur-substituted spliceosomes on a model substrate, chased spliceosomes through branching and assayed for exon ligation after affinity purification to remove ATP. Only spliceosomes containing the five sulphur substitutions implicated in branching failed to catalyse exon ligation in Mg²⁺ (Fig. 2i, m compared with 2j–l, first lanes; and data not shown). In addition to U80-PS(*S_p*) spliceosomes (Fig. 2l; ref. 28),

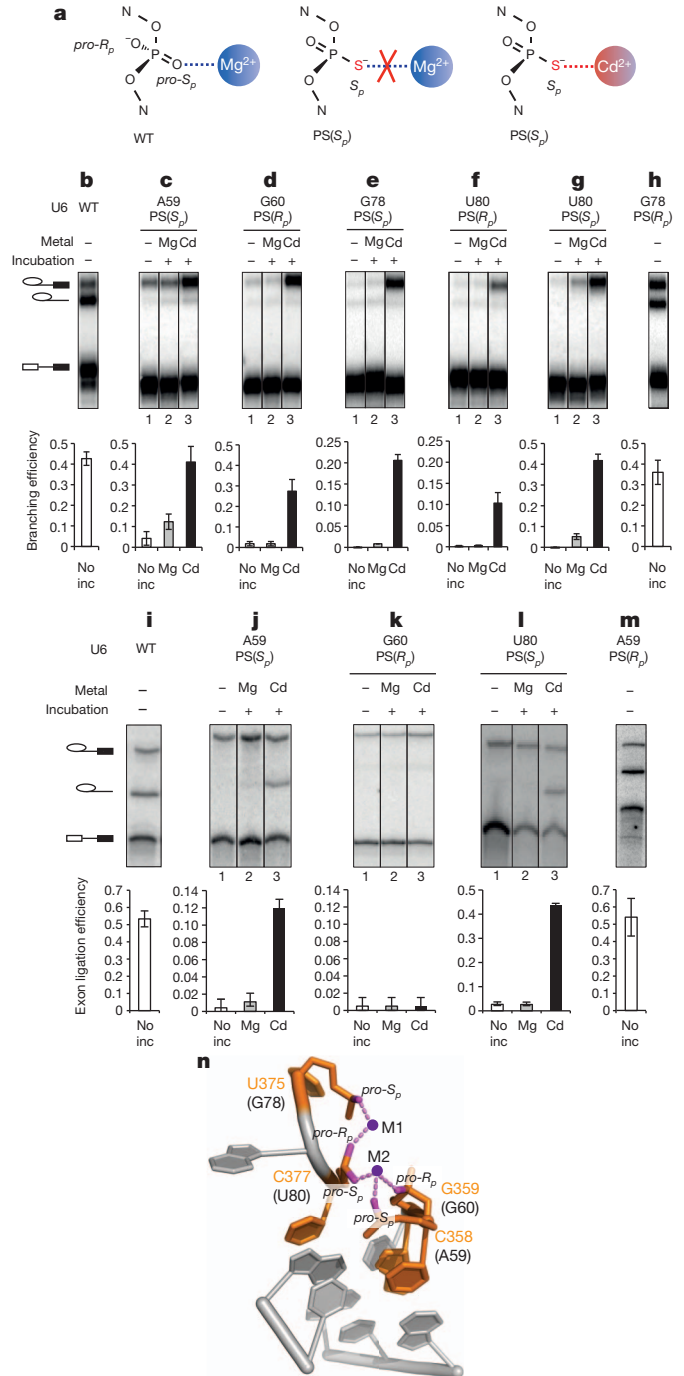


Figure 2 | U6 snRNA positions metals important for both steps of splicing. **a**, Metal rescue strategy, indicating the non-bridging oxygens that were substituted with sulphur and the consequence of a substitution for binding of Mg²⁺ or the thiophilic metal Cd²⁺. **b–m**, Cd²⁺ rescues the branching defects (**b–h**) and exon ligation defects (**i–m**) induced by specific sulphur substitutions. Values represent averages; error bars, s.d. ($n = 3$ for **b–h**; $n = 2$ for **i–m**); no inc, no incubation. **n**, Structure of the domain V metal binding core (PDB 3EOH, ref. 26). Residue numbers are shown for the group II intron, with the corresponding U6 residues in parentheses.

A59-PS(*S_p*) spliceosomes catalysed exon ligation in Cd²⁺ (Fig. 2j). Although G60-PS(*R_p*), G78-PS(*S_p*) and U80-PS(*R_p*) failed to catalyse exon ligation even in Cd²⁺ (Fig. 2k; data not shown), these sulphur substitutions exhibited more stringent requirements for metal rescue in branching, failing to tolerate the less thiophilic Mn²⁺, whereas U80-PS(*S_p*) and A59-PS(*S_p*) spliceosomes did (Extended Data Fig. 2b). Therefore the defects of these sulphur substitutions that could not be

rescued in exon ligation remain consistent with a role for the substituted oxygens as metal ligands during exon ligation (Supplementary Note 2). Thus, at least two of the oxygens that bind a metal important for branching also bind a metal important for exon ligation.

Overall, our analysis shows that five non-bridging oxygens in U6 are bona fide metal ligands in the spliceosome (Fig. 2). These ligands function after catalytic activation, implicating a structural or direct catalytic role for these ligands during the catalytic stage. These ligands correspond directly and stereospecifically to the oxygens that coordinate two divalent metals in domain V of a group II intron, as revealed by X-ray crystallography^{26,27} (Fig. 2n). This parallel suggested that the U6 ligands that function at the catalytic stage function analogously to domain V metal ligands by directly positioning the catalytic metals required for splicing.

U6 positions catalytic metals during branching

Experiments with the *Tetrahymena thermophila* group I intron have established biochemical signatures for identifying ligands that position catalytic metals: sulphur substitution of ligands to a catalytic metal can be rescued more strongly by thiophilic metal or with increased specificity for Cd^{2+} when the substrate ligands to that metal are also substituted with sulphur³¹. Consequently, to determine whether the U6 snRNA metal ligands function catalytically during branching, we first identified a substrate sensitive to the identity of catalytic metals required for branching. A pre-mRNA substrate bearing a double sulphur substitution at both the leaving group and the non-bridging *pro-R_p* oxygen at the 5' splice site (referred to as 3'S-PS(*R_p*)) was branched efficiently only in the presence of Cd^{2+} (Fig. 3a), indicating that in yeast, as in mammals²⁴ (compare with ref. 37), divalent metals interact with the scissile phosphate (see also Supplementary Notes 3 and 4 and Extended Data Figs 3 and 4). We used the 3'S-PS(*R_p*) substrate as a reporter for catalytic metal interactions between the spliceosome and the 5' splice site during branching.

These experiments revealed several catalytic interactions between U6 and the 5' splice site. Under sensitized conditions (Fig. 3 legend), the 3'S-PS(*R_p*) substrate strongly improved Cd^{2+} -mediated rescue for G78-PS(*S_p*) and U80-PS(*R_p*) spliceosomes (Fig. 3b). In contrast to the

3'S-PS(*R_p*) substrate, the 3'S-PS(*S_p*) substrate, having the *pro-S_p* oxygen, which is not directly involved in catalysis, substituted with sulphur (Extended Data Fig. 3), did not improve Cd^{2+} -mediated rescue for G78-PS(*S_p*) and U80-PS(*R_p*) (Extended Data Fig. 5a, b). These data indicate that the G78 *pro-S_p* and U80 *pro-R_p* oxygens interact with the 5' splice site through catalytic metals during branching.

The 3'S-PS(*R_p*) substrate also rescued sulphur substitutions that could not be rescued on their own. Substitution of both the *pro-S_p* and *pro-R_p* oxygens at U80 with sulphur (U80-PS₂) impaired branching of the 3'O-PO substrate, but unlike the individual substitutions, Cd^{2+} could not rescue branching (Fig. 3c). However, the 3'S-PS(*R_p*) substrate allowed robust Cd^{2+} rescue of branching for U80-PS₂ (Fig. 3c), providing evidence that both of the U80 non-bridging oxygens bind catalytic metals during branching.

The 3'S-PS(*R_p*) substrate improved rescue of these sulphur substitutions in U6 in a specific manner. The modified substrate did not improve branching for U6 variants that compromised branching due to base mutations (Extended Data Fig. 5c, d, Supplementary Note 5) and did not improve Cd^{2+} rescue for G60-PS(*R_p*) (Fig. 3b). Thus the enhanced rescue of G78-PS(*S_p*), U80-PS(*R_p*) and U80-PS₂ spliceosomes conferred specifically by the 3'S-PS(*R_p*) substrate bears the hallmark of ligands linked by common metals^{29–31} and indicates that the corresponding oxygens in U6 position catalytic metals during branching.

An implication of this conclusion is that a sulphur substitution in U6 might also reduce the Cd^{2+} concentration required for rescue of a substrate with sulphur substitutions at the 5' splice site, by enhancing Cd^{2+} occupancy of a common metal binding site. Indeed, with the 3'S-PS(*R_p*) substrate, substitution of the *pro-S_p* oxygen of U80 with sulphur decreased the Cd^{2+} titration midpoint for rescue by sixfold compared to wild-type U6 (Fig. 3d, Supplementary Note 6), and at a limiting Cd^{2+} concentration (10 μM), increased the rate of branching sevenfold compared to wild-type U6 (Extended Data Fig. 6a, b), demonstrating that U80-PS(*S_p*) increased binding of Cd^{2+} at the catalytic core.

Our analysis has also revealed that branching requires two distinct catalytic metals (compare with ref. 22). With the 3'S-PS(*R_p*) substrate, Cd^{2+} titrations indicated that rescue required binding of Cd^{2+} to two

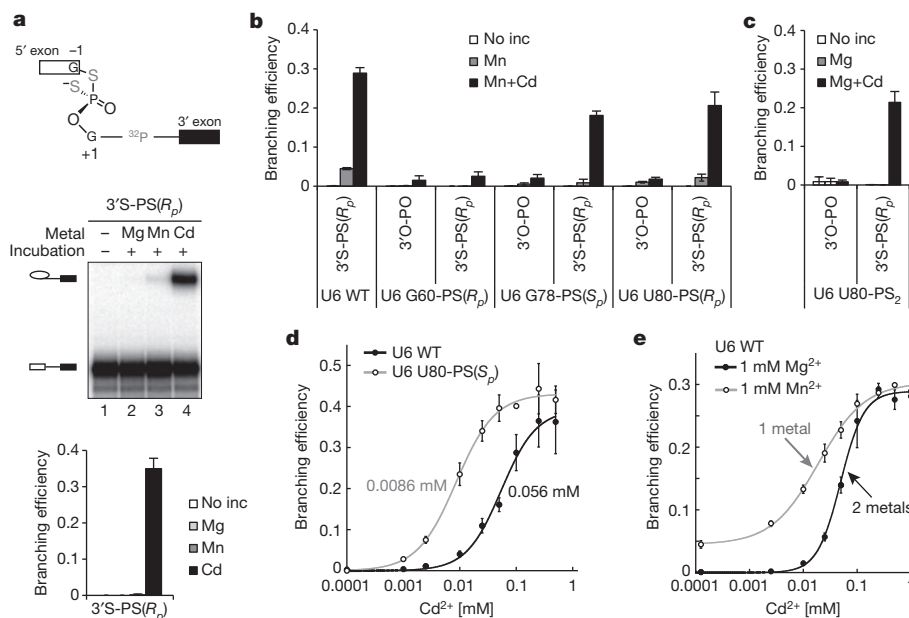


Figure 3 | U6 snRNA positions catalytic metals during branching. **a**, The 3'S-PS(*R_p*) substrate is sensitive to catalytic metal interactions. **b**, **c**, The 3'S-PS(*R_p*) substrate improves rescue of G78-PS(*S_p*), U80-PS(*R_p*) and U80-PS₂ spliceosomes. **d**, U80-PS(*S_p*) reduces the Cd^{2+} concentration required for branching of the 3'S-PS(*R_p*) substrate. **e**, The 3'S-PS(*R_p*) substrate is rescued by

Cd^{2+} bound at two distinct sites. In **d** and **e**, Hill fits are shown (solid curves); in **e**, titration midpoints are indicated. In **b** and **e**, a lower pH (pH 7.0) was used compared to Fig. 2 (pH 8.5) to sensitize the system for improved rescue. Values represent averages; error bars, s.d. ($n = 3$); no inc, no incubation.

sites, when Cd^{2+} was the only thiophilic metal present (Fig. 3e). In contrast, when Mn^{2+} was also present, rescue still required binding of Cd^{2+} but to only one site (Fig. 3e; Extended Data Fig. 7a–c), demonstrating that one metal site could bind Mn^{2+} whereas the other site could not. Given that Cd^{2+} is expected to bind a site containing several sulphur ligands, whereas Mn^{2+} is not³⁸, these and additional data indicate that one metal interacts with both sulphur atoms of the 3'-S-PS(R_p) substrate (referred to as M1) (Extended Data Fig. 7e, f), whereas the second metal only interacts with the non-bridging R_p sulphur (M2). Further evidence indicates that the U80 *pro-R_p* and G78 *pro-S_p* oxygens also interact with the M1 site, whereas the U80 *pro-S_p* oxygen interacts with the second metal site (M2) (Extended Data Figs 7 and 8, Supplementary Note 7). Thus, at least three of the five identified U6 ligands coordinate two distinct catalytic metals that interact with the scissile phosphate of the 5' splice site during branching (Supplementary Note 8, Extended Data Figs 5e–g and 6e).

U6 positions a catalytic metal during exon ligation

To determine whether the U6 metal ligands function during exon ligation by directly binding catalytic metals, we tested for biochemical signatures³¹ as above, that would link the U6 ligands to the catalytic metal that interacts with the 3' splice site during exon ligation.

First, we introduced a sulphur substitution at the 3' splice site leaving group to sensitize splicing of a model substrate to binding of the catalytic metal that interacts with this group. Additionally, we introduced a mutation of the 3' splice site consensus sequence (UAG to UAc) to stall spliceosomes before exon ligation³⁴ regardless of whether the 3'-oxygen leaving group at the 3' splice site was substituted with sulphur or oxygen (3'S or 3'O). Exon ligation of this substrate can proceed only in the absence of ATP due to proofreading³⁴. Although exon ligation of affinity-purified UAc-3'O spliceosomes proceeded in the absence of ATP, the 3'S substitution compromised exon ligation when only Mg^{2+} was present (Fig. 4a). When Mn^{2+} or Cd^{2+} was present, spliceosomes assembled on the UAc-3'S substrate catalysed exon ligation fourfold to sixfold more efficiently (Fig. 4a), indicating that a divalent metal stabilizes the leaving group in yeast, as in mammals²⁵ (see also Supplementary Note 9 and Extended Data Fig. 9a–f). Because the UAc-3'S substrate specifically required thiophilic, catalytic metals, we used it as a reporter for catalytic metal interactions between the spliceosome and the 3' splice site during exon ligation (Supplementary Note 10).

After assembling spliceosomes containing U6 sulphur substitutions on this sulphur-substituted substrate, we probed for exon ligation at the catalytic stage (that is, in the absence of ATP and soluble factors). As expected from splicing assays of the wild-type UAG-3'O substrate (Fig. 2j, l), exon ligation of the mutated UAc-3'O substrate in Mg^{2+} occurred with exceedingly low efficiency with spliceosomes containing U6 A59-PS(S_p) or U80-PS(S_p) (Fig. 4b). However, in contrast to exon ligation assays of the wild-type UAG-3'O substrate (Fig. 2j, l), exon ligation of the mutated UAc-3'O substrate by these sulphur-substituted spliceosomes was not rescued by Cd^{2+} (Fig. 4b), indicating that Cd^{2+} could no longer rescue the U6 sulphur substitutions in the context of the substrate base mutation. Nevertheless, when the substrate also contained sulphur in the leaving group position (UAc-3'S), Cd^{2+} , but not Mg^{2+} , strongly stimulated exon ligation by the sulphur-substituted spliceosomes (Fig. 4b, Extended Data Fig. 9g). This stronger rescue by Cd^{2+} of a sulphur-substituted ligand in the presence of a second sulphur-substituted ligand constitutes a signature for a functional and physical link between two ligands that bind the same metal^{29–31}. These data therefore establish that the U6 A59 *pro-S_p* and U80 *pro-S_p* oxygens interact with the catalytic metal that stabilizes the leaving group during exon ligation.

The signature was specific to the U6 A59-PS(S_p) or U80-PS(S_p) spliceosomes and was not observed for other spliceosomes that were compromised for exon ligation. Unlike the U6 sulphur-substituted spliceosomes assembled on the UAc-3'S substrate, the exon ligation

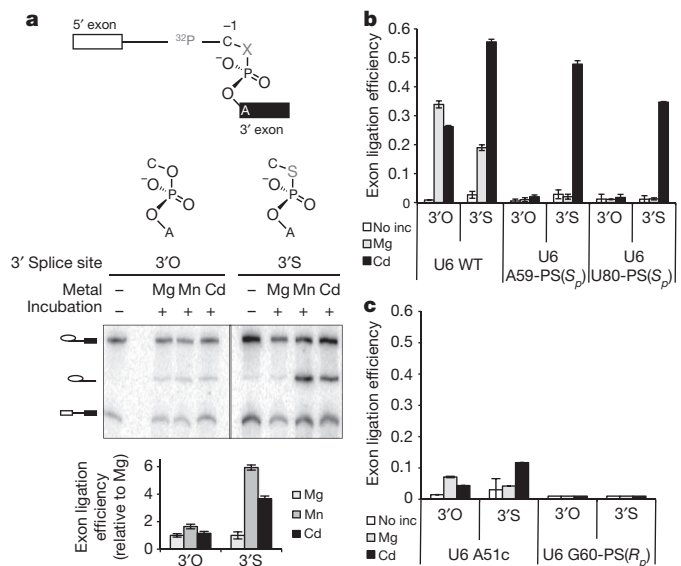


Figure 4 | U6 snRNA positions a catalytic metal during exon ligation. **a**, The UAc-3'S substrate is sensitive to catalytic metal interactions. **b**, **c**, The UAc-3'S substrate specifically improves rescue of U6 A59-PS(S_p) and U80-PS(S_p) spliceosomes. Values represent averages; error bars, s.d. ($n = 3$); no inc, no incubation.

defect³⁹ of U6 A51c spliceosomes was not substantially suppressed in Cd^{2+} by the UAc-3'S substrate (Fig. 4c). Furthermore, the exon ligation defect of G60-PS(R_p) was not suppressed by the UAc-3'S substrate in Cd^{2+} (Fig. 4c; Extended Data Fig. 9h; Supplementary Note 11), indicating that the substrate sulphur substitution alone does not enable exon ligation of compromised spliceosomes. These results and a metal specificity switch induced by U80-PS(S_p) (Extended Data Fig. 8 and Supplementary Note 12) validate the evidence that the U6 A59 *pro-S_p* and U80 *pro-S_p* oxygens interact with a catalytic metal during exon ligation.

Through a comprehensive analysis, encompassing every substrate allowed by sulphur chemistry (Extended Data Figs 5g and 9h), we have found that four of the five metal ligands in U6 position catalytic metals during the catalytic stages of splicing. Even though metal rescue strategies were insufficient to establish direct evidence linking the fifth ligand (G60 *pro-S_p*) to a splice site (Supplementary Note 2), the configuration of the RNA catalytic core implied by our data are consistent with the fifth ligand also binding a catalytic metal (see below). Importantly, at least two of the U6 metal ligands function in both steps of splicing and at least one of these, U80 *pro-S_p*, positions a catalytic metal during both branching and exon ligation (M2, Fig. 5a, b). These and other findings (Supplementary Note 13) support a model²² in which both splicing reactions are catalysed by a common, two-metal catalytic core, rather than two independent active sites, and thereby implicate a rearrangement of the substrate to sequentially accommodate mutually exclusive interactions between U6 and the 5' and 3' splice sites. Further underscoring the importance of disabling fidelity mechanisms in our approach, these results establish that the spliceosome proofreads catalytic interactions (compare with ref. 28).

Discussion

Our results indicate that the metals that mediate splicing catalysis through interactions with the scissile phosphates are bound by the spliceosome through ligands in the U6 snRNA, thus demonstrating that RNA directly mediates catalysis in the spliceosome (Fig. 5d). Notably, all of the five U6 metal ligands that function in pre-mRNA splicing (Fig. 2) correspond directly to catalytic metal ligands observed in domain V in structures of a group II intron (Figs 1b, c; 2n; 5c; refs 26, 27). Moreover, our findings imply an equivalent orientation of the substrate

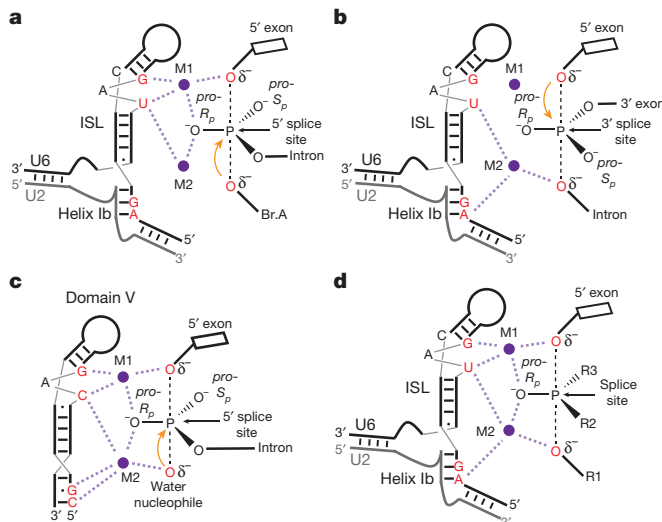


Figure 5 | Model for catalytic metal interactions during pre-mRNA splicing and comparison to the domain V catalytic core of group II introns.

a, b, Catalytic metal interactions during branching (**a**) and exon ligation (**b**). **c,** Model of domain V during hydrolysis (PDB 4FAQ, ref. 27). **d,** Two-metal model for the RNA catalytic core of the spliceosome. For branching, R1 represents the 2' hydroxyl of the branch adenosine; R2, the intron; and R3, the *pro-S_p* oxygen. For exon ligation R1 represents the 3' oxygen leaving group, R2 the *pro-S_p* oxygen; and R3 the 3' exon. Throughout the reactive oxygens are coloured red, the pre-mRNA scissile phosphate is depicted in a transition state, and interactions between specific ligands and the reactive oxygens mediated by M1 and M2 are shown as light magenta dashed lines.

relative to the metal binding core (Fig. 5a–c). Taken together, our data support a model for a single, two-metal active site (Fig. 5d; Supplementary Note 13; refs. 22, 40) and validate (compare with ref. 25) the long-standing hypothesis that the spliceosome shares a similar RNA-based catalytic core and mechanism with group II introns^{5,6,13,18,22,27,41} (Supplementary Note 14). This RNA-based mechanism is sufficient to effect metal catalysis of pre-mRNA splicing, without the need for direct protein involvement.

Given this evidence, it is noteworthy that the RNaseH-like domain of Prp8, which interacts with all reactive sites of the substrate, can bind a metal *in crystallo*⁴². Further, mutations that compromise metal binding *in crystallo* impair exon ligation, leading to the possibility that Prp8 may play a catalytic role during exon ligation⁴². Nevertheless, we have not found any evidence for a direct metal-mediated catalytic interaction between the Prp8 metal binding site and the 3' splice site (Supplementary Note 15; Extended Data Fig. 10). Thus, Prp8 may primarily promote formation of the RNA catalytic core without being a part of it; indeed, a recent structure comprising most of Prp8 has led to the suggestion that Prp8 forms a scaffold for the spliceosome's catalytic core, analogously to protein co-factors of group II introns¹⁷. A recent model of the catalytic core of the human spliceosome based on RNA structure probing and homology modelling provides further support for this interpretation^{40,43}.

Overall, our data indicate that the spliceosome, like the ribosome^{44,45}, uses RNA to effect catalysis in the context of a complex ribonucleo-protein assembly. Moreover, the common catalytic mechanism used by the spliceosome and group II introns is consistent with a common evolutionary origin between the spliceosome and these ancient RNA retroelements^{46,47}. Our findings thus support the idea that modern ribonucleoprotein enzymes evolved from a primordial 'RNA world' (ref. 48), in which catalysis was performed exclusively by RNA.

METHODS SUMMARY

U6 was depleted from *Saccharomyces cerevisiae* splicing extracts and splicing activity reconstituted with synthetic U6 snRNA, essentially as described²⁸. Spliceosomes

were assembled on modified model pre-mRNA substrates: *UBC4*, for experiments probing branching, or *ACT1*, for experiments probing exon ligation, both synthesized by splint-mediated ligation⁴⁹. Oligonucleotides containing specific 5' or 3' splice site modifications were synthesized in house, as described previously⁵⁰. Assembled spliceosomes were isolated by affinity purification via Prp19p (ref. 36), washed to remove ATP, and chased as described²⁸, at room temperature, in the absence of ATP, at pH 7.0, 8.0 or 8.5. All experiments were repeated with at least two independent extract preparations. Data were quantified using ImageQuant TL (Amersham Biosciences).

Online Content Any additional Methods, Extended Data display items and Source Data are available in the online version of the paper; references unique to these sections appear only in the online paper.

Received 15 May; accepted 3 October 2013.

Published online 6 November 2013.

- Nilsen, T. W. & Graveley, B. R. Expansion of the eukaryotic proteome by alternative splicing. *Nature* **463**, 457–463 (2010).
- Wahl, M. C., Will, C. L. & Lührmann, R. The spliceosome: design principles of a dynamic RNP machine. *Cell* **136**, 701–718 (2009).
- Sharp, P. A. On the origin of RNA splicing and introns. *Cell* **42**, 397–400 (1985).
- Cech, T. R. The generality of self-splicing RNA: relationship to nuclear mRNA splicing. *Cell* **44**, 207–210 (1986).
- Madhani, H. D. & Guthrie, C. A novel base-pairing interaction between U2 and U6 snRNAs suggests a mechanism for the catalytic activation of the spliceosome. *Cell* **71**, 803–817 (1992).
- Shukla, G. C. & Padgett, R. A. A catalytically active group II intron domain 5 can function in the U12-dependent spliceosome. *Mol. Cell* **9**, 1145–1150 (2002).
- Hilliker, A. K. & Staley, J. P. Multiple functions for the invariant AGC triad of U6 snRNA. *RNA* **10**, 921–928 (2004).
- Mefford, M. A. & Staley, J. P. Evidence that U2/U6 helix I promotes both catalytic steps of pre-mRNA splicing and rearranges in between these steps. *RNA* **15**, 1386–1397 (2009).
- Burke, J. E., Sashital, D. G., Zuo, X., Wang, Y.-X. & Butcher, S. E. Structure of the yeast U2/U6 snRNA complex. *RNA* **18**, 673–683 (2012).
- Sun, J. S. & Manley, J. L. A novel U2–U6 snRNA structure is necessary for mammalian mRNA splicing. *Genes Dev.* **9**, 843–854 (1995).
- Chanfreau, G. & Jacquier, A. Catalytic site components common to both splicing steps of a group II intron. *Science* **266**, 1383–1387 (1994).
- Fabrizio, P. & Abelson, J. Thiophosphates in yeast U6 snRNA specifically affect pre-mRNA splicing *in vitro*. *Nucleic Acids Res.* **20**, 3659–3664 (1992).
- Yu, Y. T., Maroney, P. A., Darzynkiewicz, E. & Nilsen, T. W. U6 snRNA function in nuclear pre-mRNA splicing: a phosphorothioate interference analysis of the U6 phosphate backbone. *RNA* **1**, 46–54 (1995).
- Yean, S. L., Wuenschell, G., Termini, J. & Lin, R.-J. Metal-ion coordination by U6 small nuclear RNA contributes to catalysis in the spliceosome. *Nature* **408**, 881–884 (2000).
- Gordon, P. M. & Piccirilli, J. A. Metal ion coordination by the AGC triad in domain 5 contributes to group II intron catalysis. *Nature Struct. Biol.* **8**, 893–898 (2001).
- Boudvillain, M. & Pyle, A. M. Defining functional groups, core structural features and inter-domain tertiary contacts essential for group II intron self-splicing: a NAIM analysis. *EMBO J.* **17**, 7091–7104 (1998).
- Galej, W. P., Oubridge, C., Newman, A. J. & Nagai, K. Crystal structure of Prp8 reveals active site cavity of the spliceosome. *Nature* **493**, 638–643 (2013).
- Valadkhan, S. & Manley, J. L. Splicing-related catalysis by protein-free snRNAs. *Nature* **413**, 701–707 (2001).
- Jaladat, Y., Zhang, B., Mohammedi, A. & Valadkhan, S. Splicing of an intervening sequence by protein-free human snRNAs. *RNA Biol.* **8**, 372–377 (2011).
- Smith, D. J. & Konarska, M. M. A critical assessment of the utility of protein-free splicing systems. *RNA* **15**, 1–3 (2009).
- Valadkhan, S. & Manley, J. L. The use of simple model systems to study spliceosomal catalysis. *RNA* **15**, 4–7 (2009).
- Steitz, T. A. & Steitz, J. A. A general two-metal-ion mechanism for catalytic RNA. *Proc. Natl Acad. Sci. USA* **90**, 6498–6502 (1993).
- Sontheimer, E. J., Gordon, P. M. & Piccirilli, J. A. Metal ion catalysis during group II intron self-splicing: parallels with the spliceosome. *Genes Dev.* **13**, 1729–1741 (1999).
- Sontheimer, E. J., Sun, S. & Piccirilli, J. A. Metal ion catalysis during splicing of premessenger RNA. *Nature* **388**, 801–805 (1997).
- Gordon, P. M., Sontheimer, E. J. & Piccirilli, J. A. Metal ion catalysis during the exon-ligation step of nuclear pre-mRNA splicing: extending the parallels between the spliceosome and group II introns. *RNA* **6**, 199–205 (2000).
- Toor, N., Keating, K. S., Taylor, S. D. & Pyle, A. M. Crystal structure of a self-spliced group II intron. *Science* **320**, 77–82 (2008).
- Marcia, M. & Pyle, A. M. Visualizing group II intron catalysis through the stages of splicing. *Cell* **151**, 497–507 (2012).
- Koodathingal, P., Novak, T., Piccirilli, J. A. & Staley, J. P. The DEAH box ATPases Prp16 and Prp43 cooperate to proofread 5' splice site cleavage during pre-mRNA splicing. *Mol. Cell* **39**, 385–395 (2010).
- Shan, S., Yoshida, A., Sun, S., Piccirilli, J. A. & Herschlag, D. Three metal ions at the active site of the *Tetrahymena* group I ribozyme. *Proc. Natl Acad. Sci. USA* **96**, 12299–12304 (1999).

30. Forconi, M., Lee, J., Lee, J. K., Piccirilli, J. A. & Herschlag, D. Functional identification of ligands for a catalytic metal ion in group I introns. *Biochemistry* **47**, 6883–6894 (2008).
31. Frederiksen, J. K. & Piccirilli, J. A. Identification of catalytic metal ion ligands in ribozymes. *Methods* **49**, 148–166 (2009).
32. Guo, F., Gooding, A. R. & Cech, T. R. Structure of the *Tetrahymena* ribozyme: base tripartite sandwich and metal ion at the active site. *Mol. Cell* **16**, 351–362 (2004).
33. Burgess, S. M. & Guthrie, C. A mechanism to enhance mRNA splicing fidelity: the RNA-dependent ATPase Prp16 governs usage of a discard pathway for aberrant lariat intermediates. *Cell* **73**, 1377–1391 (1993).
34. Mayas, R. M., Maita, H. & Staley, J. P. Exon ligation is proofread by the DExD/H-box ATPase Prp22p. *Nature Struct. Mol. Biol.* **13**, 482–490 (2006).
35. Semlow, D. R. & Staley, J. P. Staying on message: ensuring fidelity in pre-mRNA splicing. *Trends Biochem. Sci.* **37**, 263–273 (2012).
36. Chan, S.-P., Kao, D.-I., Tsai, W.-Y. & Cheng, S.-C. The Prp19p-associated complex in spliceosome activation. *Science* **302**, 279–282 (2003).
37. Moore, M. J. & Sharp, P. A. Evidence for two active sites in the spliceosome provided by stereochemistry of pre-mRNA splicing. *Nature* **365**, 364–368 (1993).
38. Pecoraro, V. L., Hermes, J. D. & Cleland, W. W. Stability constants of Mg²⁺ and Cd²⁺ complexes of adenine nucleotides and thionucleotides and rate constants for formation and dissociation of MgATP and MgADP. *Biochemistry* **23**, 5262–5271 (1984).
39. Fabrizio, P. & Abelson, J. J. Two domains of yeast U6 small nuclear RNA required for both steps of nuclear precursor messenger RNA splicing. *Science* **250**, 404–409 (1990).
40. Anokhina, M. *et al.* RNA structure analysis of human spliceosomes reveals a compact 3D arrangement of snRNAs at the catalytic core. *EMBO J.* **32**, 2804–2818 (2013).
41. Cech, T. R. The chemistry of self-splicing RNA and RNA enzymes. *Science* **236**, 1532–1539 (1987).
42. Schellenberg, M. J. *et al.* A conformational switch in PRP8 mediates metal ion coordination that promotes pre-mRNA exon ligation. *Nature Struct. Mol. Biol.* **20**, 728–734 (2013).
43. Bonnal, S. & Valcárcel, J. RNAtomy of the spliceosome's heart. *EMBO J.* **32**, 2785–2787 (2013).
44. Nissen, P., Hansen, J., Ban, N., Moore, P. B. & Steitz, T. A. The structural basis of ribosome activity in peptide bond synthesis. *Science* **289**, 920–930 (2000).
45. Beringer, M. & Rodnina, M. V. The ribosomal peptidyl transferase. *Mol. Cell* **26**, 311–321 (2007).
46. Sharp, P. A. Five easy pieces. *Science* **254**, 663 (1991).
47. Martin, W. & Koonin, E. V. Introns and the origin of nucleus–cytosol compartmentalization. *Nature* **440**, 41–45 (2006).
48. Joyce, G. F. The antiquity of RNA-based evolution. *Nature* **418**, 214–221 (2002).
49. Moore, M. J. & Sharp, P. Site-specific modification of pre-mRNA: the 2'-hydroxyl groups at the splice sites. *Science* **256**, 992–997 (1992).
50. Yoshida, A., Sun, S. & Piccirilli, J. A. A new metal ion interaction in the *Tetrahymena* ribozyme reaction revealed by double sulfur substitution. *Nature Struct. Biol.* **6**, 318–321 (1999).

Supplementary Information is available in the online version of the paper.

Acknowledgements We thank C. Guthrie for plasmids; S.-C. Cheng for anti-Cwc25p serum; D. Semlow for strains; J. Olvera for reagents and experimental assistance; R.-J. Lin for sharing unpublished data; members of the Staley and Piccirilli laboratories for discussions; and D. Herschlag, A. Macmillan and T. Nilsen for comments on the manuscript. N.T. was supported by an NSF Graduate Research Fellowship and by a CBI Training Grant (5T32GM008720). This work was funded by a grant from the Chicago Biomedical Consortium, with support from The Searle Funds at the Chicago Community Trust, to J.P.S., A. S. Mankin and E. J. Sontheimer, and by a grant from the National Institutes of Health (R01GM088656) to J.P.S. and J.A.P.

Author Contributions S.M.F., N.T., T.N., J.P.S. and J.A.P. designed the study; T.N. and P.K. performed initial screening of U6 sulphur substitutions; S.M.F. performed all experiments related to branching; N.T. performed all experiments related to exon ligation; S.M.F. and N.T. together performed Prp8p experiments; J.L., N.-S.L. and Q.D. synthesized RNA oligonucleotides; S.M.F., N.T., J.P.S. and J.A.P. analysed the data and wrote the manuscript.

Author Information Reprints and permissions information is available at www.nature.com/reprints. The authors declare no competing financial interests. Readers are welcome to comment on the online version of the paper. Correspondence and requests for materials should be addressed to J.A.P. (jpicciri@uchicago.edu) or J.P.S. (jstaley@uchicago.edu).

METHODS

Strains. Experiments probing branching were performed using *S. cerevisiae* strain yJPS1405, which was derived from BY4741 (*MATa his3Δ1 leu2Δ0 met15Δ0 ura3Δ0*, Open Biosystems), by integrating a biotinylation signal C-terminal to the *PRP19* locus using *KanMX6* as a selective marker; the integration fragment, including the biotinylation signal, an ADH1 terminator, and the *KanMX* sequences were amplified from pFA6-HTB-*KanMX* (ref. 51).

Experiments probing exon ligation were performed using the previously described *S. cerevisiae* strain yJPS860 containing a C-terminal TAP tag on Prp19 (ref. 34).

Experiments involving Prp8 were performed using *S. cerevisiae* strains yJPS1471 (*PRP8* wild-type) and yJPS1472 (*PRP8* D1853C), both derived from yJPS860 (ref. 34). Briefly, the entire coding sequence of *PRP8* was replaced in yJPS860 with *LEU2*, after transformation with *PRP8* on a *URA3* plasmid (bJPS1874), yielding yJPS1470. Then yJPS1471 and 1472 were derived from yJPS1470 by plasmid shuffle on 5-FOA after transformation with bJPS2263 (*PRP8* wild-type on a *HIS3* plasmid, same as pJU186, ref. 52) or bJPS2589 (*PRP8* D1853C). bJPS2589 was derived from pJU186 (ref. 52) by QuikChange mutagenesis and confirmed by sequencing.

Pre-mRNA splicing substrates. Branching experiments were performed using *UBC4* pre-mRNA⁵³ truncated at the 5' and 3' ends down to 20 nucleotide exons. Exon ligation experiments were performed using *ACT1* pre-mRNA. Pre-mRNA substrates were prepared by splint-mediated ligation⁴⁹ using T4 RNA ligase 2 (NEB) or T4 DNA ligase (in house).

Oligonucleotides UBC4-5'E, 5'E2, UBC4-M, and UBC4-M1 were purchased from Dharmacon. Oligonucleotide UBC4M2, bearing various modifications, was synthesized in house⁵⁰ and purified by HPLC on a DNAPac P-100 column using the Waters 2795 system⁵⁴. Oligonucleotides ACT1-3'O-pc, ACT1-3'S-pc, ACT1-UAc-3'O, and ACT1-UAc-3'S were synthesized in house. The correct identity (position and chirality) of specific sulphur modifications was verified by mass spectrometry, silver or iodine cleavage, and analytical T1 digestion⁵⁵ (data not shown). Oligos M, M1, and M2 were phosphorylated with unlabelled ATP before ligation. The UBC4-TX transcript was synthesized by *in vitro* transcription using a PCR-derived template that started transcription at position +37 of the intron and ended at the last nucleotide of the exon; the template was generated using primers T7 UBC4 37-135 F and HindIII UBC4 R. The transcript was gel purified, treated with calf inorganic phosphatase (NEB), and 5' phosphorylated with [γ -³²P]ATP (Perkin Elmer, 6,000 C mmol⁻¹) before ligation.

The ACT1-5'-end plasmid was constructed by stepwise PCR from plasmid pJPS149 (ref. 34) to generate a DNA template containing an EcoRI site, the T7 promoter, ACT1 nucleotides 1–373, an HDV ribozyme sequence⁵⁶ and a HindIII site. The template was then cloned into vector pUC19. The ACT1-1-373 transcript was synthesized by *in vitro* transcription from the ACT1-5'-piece plasmid linearized with HindIII. In cases where HDV cleavage was inefficient during transcription, the RNA was resuspended in 10 mM Tris (pH 7.5) and 20 mM MgCl₂. Ribozyme cleavage was induced by 2–4 cycles of 90 °C for 1 min, room temperature for 15 min and 37 °C for 15 min. The buffer conditions were then adjusted for T4 PNK (NEB) treatment of the transcript to remove the 2'-3'-cyclic phosphate left by the ribozyme. The ACT1-392–590 transcript was synthesized by *in vitro* transcription using a PCR-derived template generated using plasmid bJPS149 (ref. 34). As the subsequent ligation requires a 5'-monophosphate group, a fourfold excess of GMP over GTP was included in the transcription reaction.

For a typical *UBC4* ligation reaction, 20 pMol of UBC4 5'E, 10 pMol of UBC4 M, M1, or M2 and 20 pMol of UBC4 TX were hybridized to 10 pMol of UBC4 splint in buffer TEN (10 mM Tris-HCl, pH 7.5; 1 mM EDTA; 66 mM NaCl) on a thermal cycler by heating to 90 °C for 2 min followed by reduction of the temperature by 1 °C for 1 min in 72 sequential steps, to a final temperature of 18 °C. T4 RNA ligase 2 (10–20 U) was then added and reactions were incubated at 37 °C for 6 h. Ligated, full-length *UBC4* pre-mRNA was purified on an 8% denaturing polyacrylamide gel and recovered by passive elution in TE buffer at 4 °C overnight (10 mM Tris-HCl pH 7.5; 1 mM EDTA).

For a typical *ACT1* ligation reaction, 500 pMol of ACT1-1-373, 50 pMol of oligonucleotide ACT1-3'O and 500 pMol of ACT1-392-590 were hybridized to 50 pMol of ACT1 splint in buffer TEN₅₀ (10 mM Tris-HCl, pH 7.5; 1 mM EDTA; 50 mM NaCl) on a thermal cycler by heating to 90 °C for 2 min followed by reduction of the temperature by 1 °C for 1 min to 24 °C, then cooling to 4 °C for 5 min. T4 DNA ligase (~100 pMol, synthesized in house) was then added and reactions were incubated at 37 °C for 4 h. The ligation reactions were DNase treated (RNase-free DNase, Promega) for 15 min to remove splint, phenol-chloroform extracted and ethanol precipitated before purification on 6% denaturing polyacrylamide gel. Bands containing full-length *ACT1* pre-mRNA were excised and recovered by passive elution in TEN₂₅₀ buffer (10 mM Tris-HCl pH 7.5, 1 mM EDTA, 250 mM NaCl) overnight at 4 °C.

Splicing extracts and U6 depletion and reconstitution. Splicing extracts were prepared using the liquid nitrogen method, as described⁵². U6 depletion and reconstitution was performed essentially as described²⁸, with the following modifications. The U6 d1 oligonucleotide was titrated for each extract to optimize depletion and reconstitution of U6; typically, 0.8 μM U6 d1 was optimal. After depletion of U6, to promote degradation of the U6 d1 oligonucleotide before addition of the synthetic U6, DNase I (Ambion, 0.05 U μl⁻¹ final) was added together with the glucose used to deplete ATP. Additionally, to ensure complete inactivation of the U6 d1 oligonucleotide, an oligonucleotide antisense to U6 d1 (U6 αd1, 0.3 μM final)⁵⁷ was added immediately before reconstitution and incubated on ice for 5 min. For reconstitution U6 was added back to a final concentration of 0.2–0.3 μM. Modified U6 was constructed by splint-mediated ligation essentially as described²⁸. Wild-type U6 was synthesized by *in vitro* transcription according to standard procedures using pJPS488 linearized with DraI as template⁵⁸. There was no difference in splicing efficiency between spliceosomes reconstituted with wild type U6 made by ligation or by *in vitro* transcription (data not shown and Extended Data Fig. 6b).

In vitro splicing. *In vitro* splicing was performed essentially as described²⁸ using ³²P-labelled substrates (0.2–0.4 nM). In Fig. 2c, g, extracts were pre-incubated with 2 mM EDTA at 4 °C for 30 min before assembling the reactions; MgCl₂ was adjusted to 3.3 mM during the splicing reaction (compared to standard 2.5 mM) to compensate for the final EDTA concentration (0.8 mM). Reactions were usually incubated in extract for 25 min before affinity purification of assembled complexes, except for experiments in Fig. 3a and Extended Data Fig. 3, where initial incubation was performed for 10 min. Assembled and stalled complexes were affinity-purified, via tagged Prp19p, by incubating the splicing reactions for 1–3 h at 4 °C with a 10%–20% reaction volume of streptavidin-agarose (Thermo Scientific) or IgG-Sepharose (GE) slurry pre-washed twice with 25–50 volumes of IPP₁₅₀ (10 mM Tris-HCl pH 8.0; 150 mM NaCl; 0.01% NP-40 substitute (Fluka)). Following immunoprecipitation, beads were washed at 4 °C twice with 50 volumes of buffer PK (3% PEG₈₀₀₀, 60 mM potassium phosphate, pH 7.0), and spliceosomes were assayed for splicing in the absence of ATP (except where noted), in buffer PK (pH 7.0, 8.0, or 8.5, as indicated) with various amounts of the indicated metals and EDTA (where noted) at room temperature (23–24 °C) with constant rotation, for 60 to 90 min. Metal solutions were prepared from corresponding powdered salts of at least 99.99% purity (Sigma).

Affinity-purified spliceosomes were incubated as follows. In Figs 2c and 3a – buffer PK (pH 8.5, with 0.5 mM EDTA) with 1 mM MgCl₂ and 1 mM of the indicated metals; in Fig. 2d–g, buffer PK (pH 8.5) with 0.5 mM MgCl₂ and 0.5 mM of the indicated metals; in Figs 2j–l and 4b, c, buffer PK (pH 7.0) with 2 mM MgCl₂ and 0.1 mM CdCl₂; in Fig. 2k, l spliceosomes containing A59-PS(S_p) and U80-PS(S_p) were chased through branching in the presence of 0.1 mM CdCl₂ before affinity purification. In Fig. 3b, e, buffer PK (pH 7.0) with 1 mM MnCl₂ alone or in combination with 1 mM CdCl₂; in Fig. 3c, buffer PK (pH 8.5) with 0.5 mM MgCl₂ and 0.5 mM CdCl₂; in Fig. 3d, buffer PK (pH 8.5) with 0.5 mM MgCl₂ and various amounts of CdCl₂, as indicated. In Fig. 4a, buffer PK (pH 7.0) with 1 mM MgCl₂ and 0.1 mM CdCl₂ or 0.1 mM MnCl₂.

Following *in vitro* splicing, products were separated on 15% denaturing polyacrylamide gels for *UBC4* substrates or 6% denaturing polyacrylamide gels for *ACT1* substrates. All experiments were repeated with at least two independent extract preparations.

Cwc25p depletion and reconstitution. For depletion of Cwc25p, splicing extracts were prepared fresh, dialysed against buffer D (ref. 52), and then incubated at 4 °C for 1.5 h with 50% volume equivalent of protein A-sepharose (Sigma) (1:1 slurry in IPP₁₅₀) conjugated to anti-Cwc25 serum (gift from S. -C. Cheng, ref. 59) and pre-equilibrated in buffer D by rotation at 4 °C for 15 min. Beads were removed by centrifugation at 800g for 4 min and the supernatant was used as depleted extract.

rCwc25p extended with a C-terminal six-histidine tag was expressed in *E. coli* BL21(DE3)pLysS transformed with pET15b (ref. 59; a gift from S. -C. Cheng). Induction in *E. coli* and purification by Ni²⁺-NTA affinity chromatography were performed essentially as described⁶⁰ but binding and washing was performed manually. Following elution from the Ni²⁺-NTA resin, the protein was further purified by glycerol gradient centrifugation to more than 90% purity (as estimated by Coomassie blue staining).

To prepare the heat-soluble extract fraction (HP), yeast splicing extracts were incubated at 90 °C for 5 min and insoluble material was removed by centrifugation at 16000g for 5 min. The supernatant was used as HP.

For complementation of affinity purified spliceosomes from extracts immunodepleted of Cwc25p, spliceosomes were washed twice with 50 volumes of buffer DK (20 mM HEPES-KOH, pH 7.9; 60 mM potassium phosphate, pH 7.0; 50 mM NaCl; 0.2 mM EDTA) and splicing was assayed in buffer DK, in the presence of rCwc25-6His (0.7–1.4 μM) and a heat soluble extract fraction (HP; typically 1–2 μl for a 50 μl splicing reaction).

To determine the rates of branching in Extended Data Fig. 4d, reactions were pre-incubated with rCwc25p and HP in the absence of metal at room temperature for 5 min to allow binding and temperature equilibration. Splicing was initiated by addition of metals; aliquots were removed at various times, immediately quenched in STOP buffer (50 mM NaOAc, pH 5.2; 1 mM EDTA; 0.1% SDS; 0.1 mg ml⁻¹ glycogen) and placed on ice before phenol extraction.

Oligonucleotides. The following oligonucleotides were used for synthesis of *UBC4* substrates. UBC4 5'E: 5'-GAACUAAGUGAUCUAGAAAGG-3'; UBC4 5'Ev2: 5'-GAACUAAGUGAUCUA-3'; UBC4 M: 5'-UAUGUCUAAAGUU AU-3'; UBC4 M1: 5'-GAAAG(3'S)GUAUGUCUAAAGUUU-3'; UBC4 M2: 5'-GAAAG(3'S-PS)GUAUGUCUAAAGUUU-3'; UBC4 Splint: 5'-CACGCA TTTGAAACGTGGCCATAACTTTAGACATACCTTTCTAGATCACTTATTC-3' (ligation splint); T7 UBC4 37-135 F: 5'-TAATACGACTCACTATAGGCCACG TTTCAATGC-3' (forward primer to generate the template UBC4 TX); HindIII UBC4 R: 5'-ATAAGCTTAACATGAAGTAGGTGGATCTC-3' (reverse primer to generate the template for UBC4 TX).

The following oligonucleotides were used for synthesis of *ACT1* substrates. ACT1-3'O-pc: 5'-UUUA(2'-*o*-nitrobenzyl-G)AGGUUGCUGCUUU-3'; ACT1-3'S-pc: 5'-UUUA(3'S, 2'-*o*-nitrobenzyl-G)AGGUUGCUGCUUU-3'; ACT1-UAc-3'O: 5'-UUUACACGUUGCUGCUUU-3'; ACT1-UAc-3'S: 5'-UUUA(3'S-C)AG GUUGCUGCUUU-3'; ACT1-UAc-splint: 5'-GAACCGTTATCAATAACCAAA GCAGCAACGTGTAAACATATAATATAGCAACAAAA-3'; ACT1-splint: 5'-G AACCGTTATCAATAACCAAAAGCAGCAACCTCTAAACATATAATATAGCA AAAAA-3'; act1-3'-end-for-1: 5'-TAATACGACTCACTATAGGTTATTGAT AACGGTTATTG-3' (forward DNA primer to generate ACT1 392–590 transcription template); act1-3'-end-for-2: 5'-GAAATTAATACGACTCACTATAGGTT ATTG-3' (forward DNA primer to generate ACT1 392–590 transcription template); act1-3'-end-rev: 5'-mUmUGGGCTGCAGGTGCAGCTC-3' (reverse DNA primer to generate ACT1 392–590 transcription template); EcoRI+T7:5'-AGTG AATTCCTTAATACGACTCACTATAGG-3' (forward DNA primer to generate ACT1 1-373-HDV template); Forward long: 5'-CGTAATACGACTCACT ATAGGGCGAATTGG-3' (forward DNA primer to generate ACT1 1-373-HDV template); Reverse-A-25: 5'-CGAGGAGGCTGGGAGCATGCCGGCCATAT AATATAGCAACAAAAAGAAT-3' (reverse DNA primer to generate ACT1 1-373-HDV template); Reverse 0-50: 5'-CCGGAATGTTGCCAGCCGGCGC CGCGAGGAGGCTGGGAGCATGCCGGCC-3' (reverse DNA primer to generate ACT1 1-373-HDV template); Reverse 25-75: 5'-GTGCGTCCCATTGCCATT ACCGGACGGTCCGGAATGTTGCCAGCCGGCGCCG-3' (reverse DNA primer to generate ACT1 1-373-HDV template); Reverse final: 5'-GTGCGTCCCATTCCG CCATTACCCG-3' (reverse DNA primer to generate ACT1 1-373-HDV template).

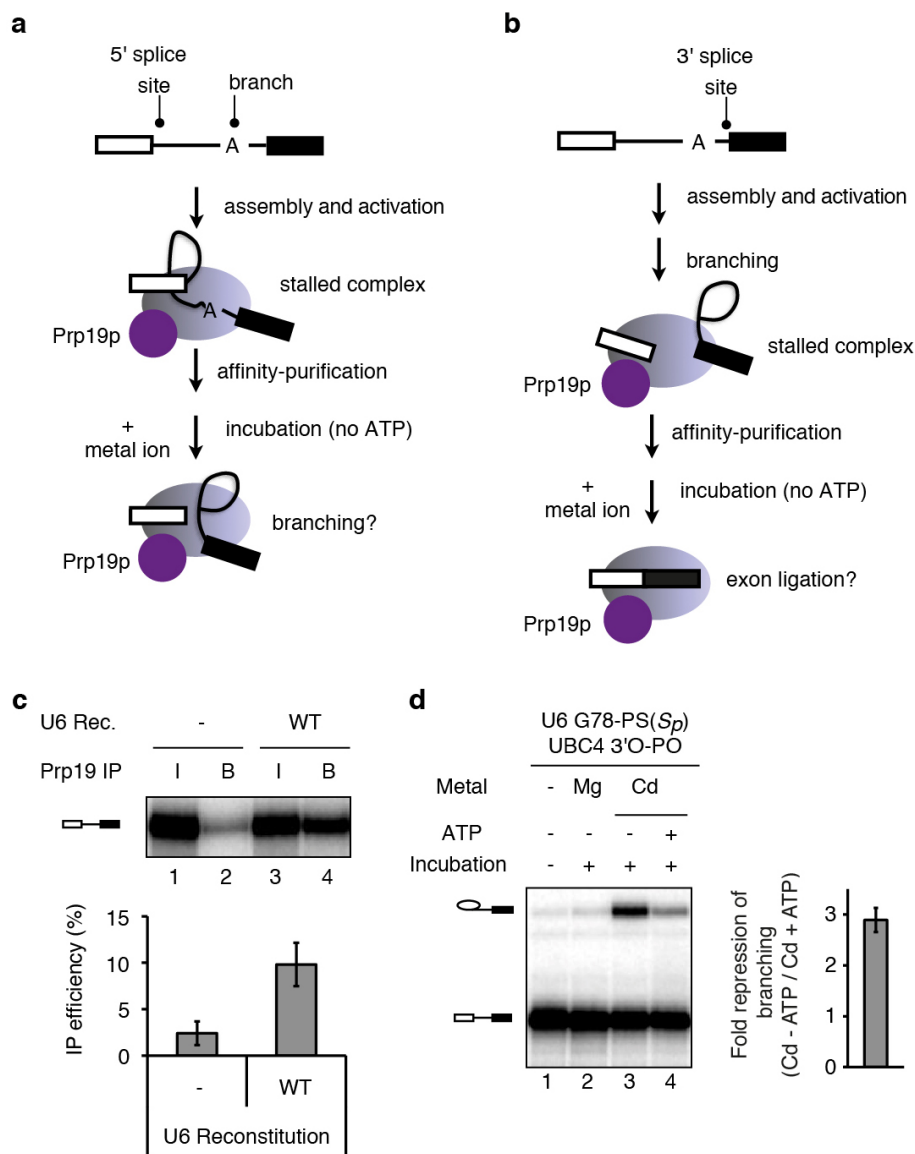
Data analysis. Gels were dried, exposed to storage phosphor screens (Amersham Biosciences) for 24 to 48 h, and scanned using a Typhoon Trio phosphorimager (Amersham Biosciences). Bands were quantified using ImageQuant TL with an automated rolling ball algorithm for background subtraction. The efficiency of branching was calculated as $LI/(LI + P)$, if EI represented less than 1% of all species or $(LI + EI)/(LI + EI + P)$ in all other cases; LI, lariat intermediate; EI,

excised intron; P, pre-mRNA. The efficiency of exon ligation was calculated as $EI/(EI + LI)$.

The rescue midpoint for the metal titration curves in Fig. 3d and Extended Data Fig. 6c,d was obtained by fitting the rescue profiles to the general Hill equation $A = A_{\max}x^n/(x^n + K^n)$, where A_{\max} is the splicing efficiency at saturation, K is the rescue midpoint, x is the CdCl₂ concentration, and n is the Hill coefficient. Curves in Fig. 3e and Extended Data Fig. 7a were fit to the following equations: $y = E_0 + Ex/(x + K_{Cd})$ (1 metal model) or $y = E_0 + Ex^2/(x^2 + K_{Cd}^2)$ (2 metal model), where y is the branching efficiency, E_0 is the extent of branching in the absence of Cd²⁺, E is the extent of branching at saturating Cd²⁺, and K_{Cd} is the apparent transition midpoint for Cd²⁺ binding. Fits using the general Hill equation: $y = E_0 + Ex^n/(x^n + K_{Cd}^n)$, where n is the number of metal sites titrated, gave the same number of sites (within fit error) as those assuming a fixed n (data not shown).

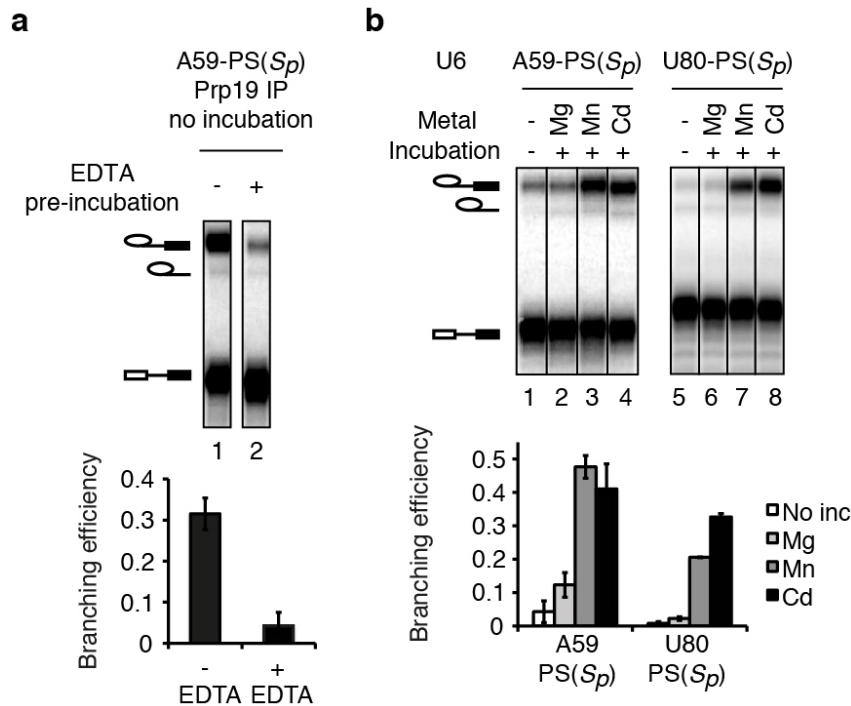
Initial rates in Extended Data Figs 4d and 6a, b were obtained by fitting the linear portion of the splicing time courses to the equation $A = A_0 + k_{\text{initial}}t$, where A is the splicing efficiency at time t and A_0 is the extent of splicing at time 0. Rates in Extended Data Fig. 9 were obtained by fitting the splicing time courses to the equation $E = E_0 + A(1 - e^{-kt})$ where E is the extent of reaction, E_0 is the extent at time = 0, A is the amplitude, k is the rate of reaction, and t is the time in minutes.

- Tagwerker, C. *et al.* HB tag modules for PCR-based gene tagging and tandem affinity purification in *Saccharomyces cerevisiae*. *Yeast* **23**, 623–632 (2006).
- Umen, J. G. & Guthrie, C. A novel role for a U5 snRNP protein in 3' splice site selection. *Genes Dev.* **9**, 855–868 (1995).
- Abelson, J., Hadjivassiliou, H. & Guthrie, C. Preparation of fluorescent pre-mRNA substrates for an smFRET study of pre-mRNA splicing in yeast. *Methods Enzymol.* **472**, 31–40 (2010).
- Frederiksen, J. K. & Piccirilli, J. A. Separation of RNA phosphorothioate oligonucleotides by HPLC. *Methods Enzymol.* **468**, 289–309 (2009).
- Loverix, S., Winqvist, A., Strömberg, R. & Steyaert, J. Mechanism of RNase T1: concerted triester-like phosphoryl transfer via a catalytic three-centered hydrogen bond. *Chem. Biol.* **7**, 651–658 (2000).
- Schürer, H., Lang, K., Schuster, J. & Mörl, M. A universal method to produce *in vitro* transcripts with homogeneous 3' ends. *Nucleic Acids Res.* **30**, e56 (2002).
- Dery, K. J., Yean, S.-L. & Lin, R.-J. Assembly and glycerol gradient isolation of yeast spliceosomes containing transcribed or synthetic U6 snRNA. *Methods Mol. Biol.* **488**, 41–63 (2008).
- Fabrizio, P., McPheeters, D. S. & Abelson, J. *In vitro* assembly of yeast U6 snRNP: a functional assay. *Genes Dev.* **3**, 2137–2150 (1989).
- Chiu, Y.-F. *et al.* Cwc25 is a novel splicing factor required after Prp2 and Yju2 to facilitate the first catalytic reaction. *Mol. Cell. Biol.* **29**, 5671–5678 (2009).
- Warkocki, Z. *et al.* Reconstitution of both steps of *Saccharomyces cerevisiae* splicing with purified spliceosomal components. *Nature Struct. Mol. Biol.* **16**, 1237–1243 (2009).
- Sigel, R. K. O., Song, B. & Sigel, H. Stabilities and structures of metal ion complexes of adenosine 5'-*O*-thiomonophosphate (AMPS²⁻) in comparison with those of its parent nucleotide (AMP²⁻) in aqueous solution. *J. Am. Chem. Soc.* **119**, 744–755 (1997).



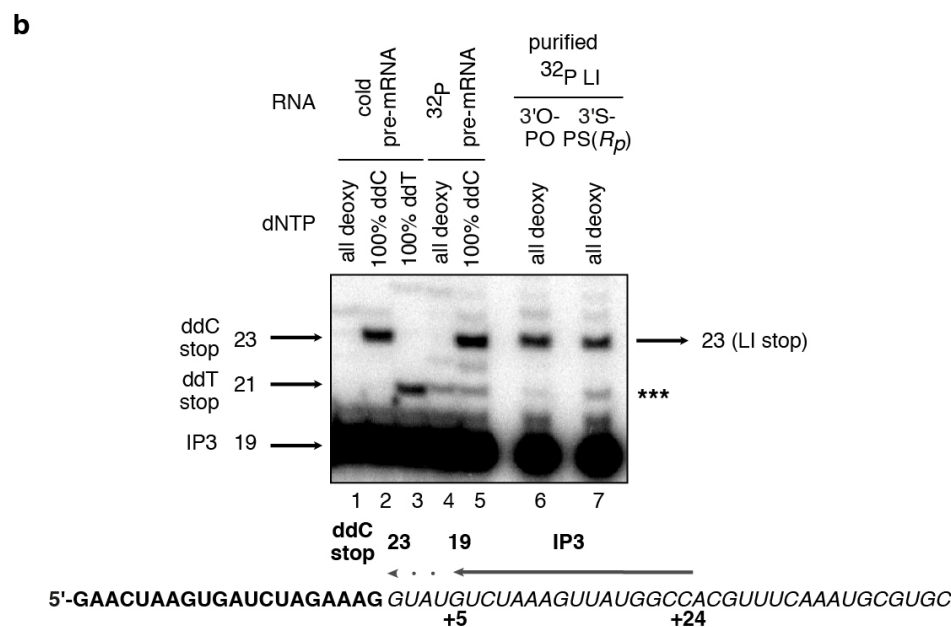
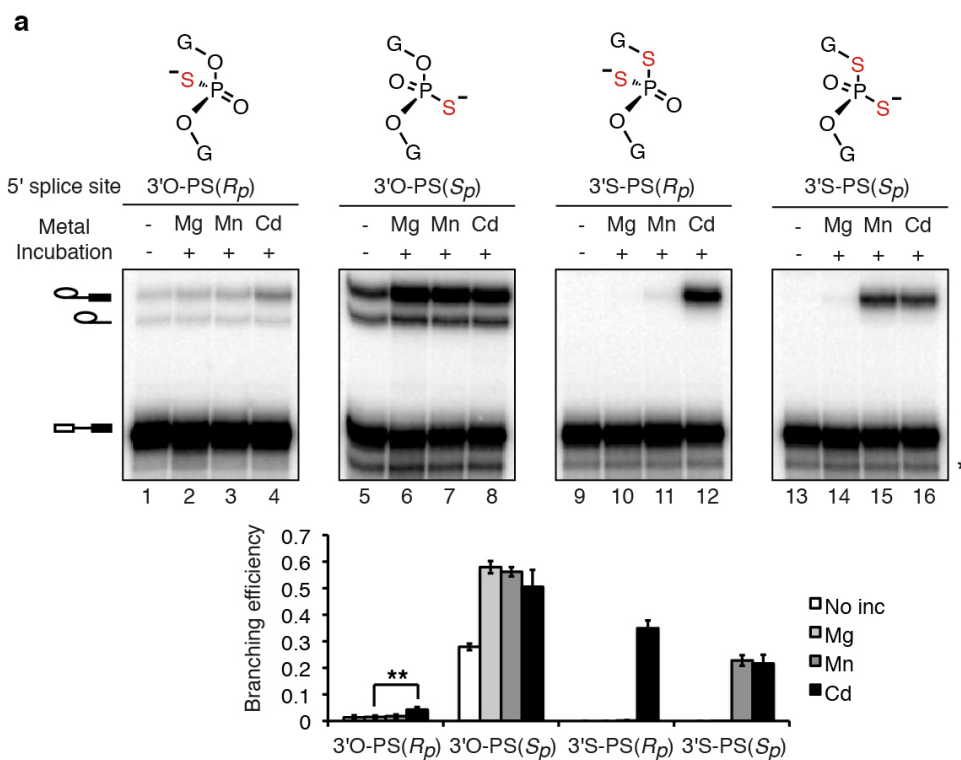
Extended Data Figure 1 | Affinity purification of spliceosomes with Prp19 requires reconstitution with U6 snRNA and enhances the potential to detect rescue by thiophilic metals. **a, b,** Schemes depicting experimental strategy for staging spliceosomes to monitor branching (**a**) or exon ligation (**b**) in the absence of ATP. Spliceosomes are depicted as light magenta ovals and Prp19p as a magenta circle. Following affinity purification of spliceosomes by Prp19p (ref. 36), beads were washed to remove ATP and soluble factors and metals ions were added to assay for splicing. **c,** Prp19p-mediated affinity purification of activated spliceosomes, reflected by immunoprecipitation of pre-mRNA, is specific for properly reconstituted complexes. Note that the affinity

purification allows quantification of the branching efficiency for activated complexes, independently of any effects on assembly. RNA from 10% of the reaction (input, I) or from beads after affinity purification (B) was extracted and analysed by denaturing PAGE. Raw data (top); quantification of immunoprecipitation efficiency (bottom); Rec., reconstitution. **d,** ATP represses the Cd²⁺ rescue for G78-PS(*S_p*) spliceosomes. Spliceosomes were assayed as in Fig. 2e; for lane 4, 2 mM ATP-Mg²⁺ was also present during the incubation. Representative gel (left) and quantification of the extent of ATP repression (right). Values are averages; error bars represent s.d. ($n = 3$).



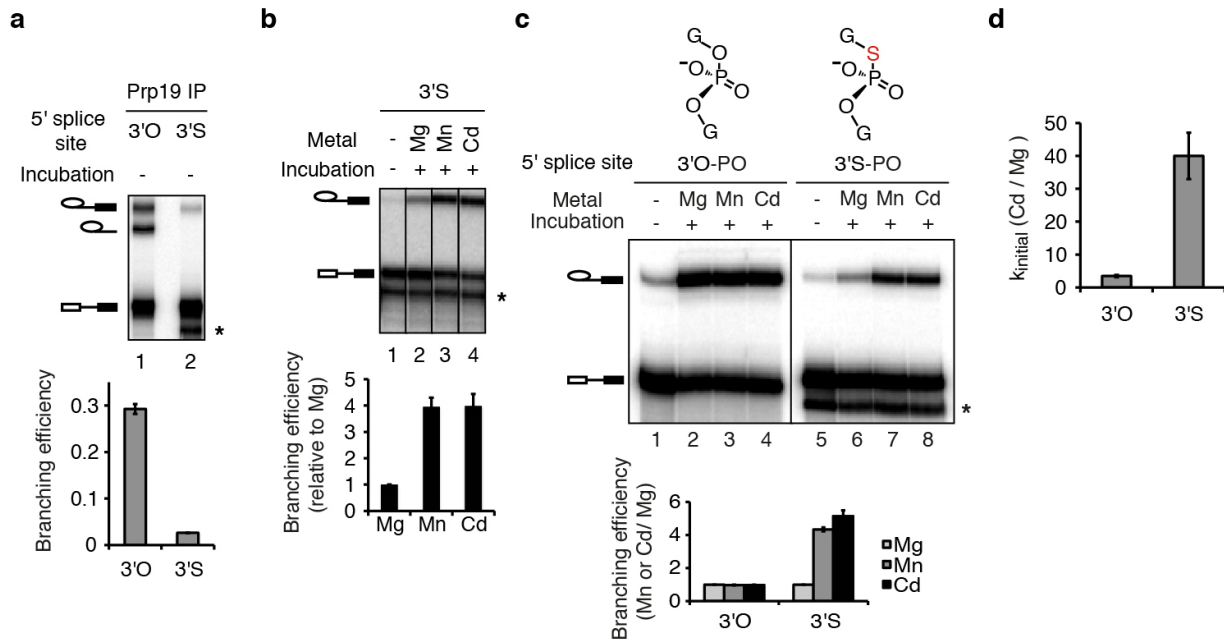
Extended Data Figure 2 | Broad rescue specificity of A59-PS(S_p) and U80-PS(S_p) spliceosomes. **a**, Pre-incubation with EDTA reveals a branching defect for A59-PS(S_p). Extracts were pre-incubated at 4 °C in the presence or absence of 2 mM EDTA and then incubated with the 3' O substrate. After affinity-purification, branching efficiency was quantified without further incubation (bottom). A representative gel is shown (top). EDTA pre-incubation caused an eightfold reduction in branching efficiency, indicating that splicing extracts may contain a thiophilic metal that supports branching by A59-PS(S_p) spliceosomes; note that pre-mRNA still immunoprecipitated efficiently, indicating catalytic activation of the spliceosome. In contrast EDTA pre-incubation has no effect on U6 wild-type spliceosomes (data not shown). **b**, The

branching defects for A59-PS(S_p) and U80-PS(S_p) spliceosomes are rescued by either Mn^{2+} or Cd^{2+} . Assays were as in Fig. 2c. A representative gel (top) and quantification (bottom) are shown; no inc, no incubation. Both Mn^{2+} and Cd^{2+} strongly rescue A59-PS(S_p) and U80-PS(S_p) spliceosomes (lanes 3, 4, 7 and 8), suggesting that even the weaker Mn^{2+} -S interaction³⁸ at these positions can support branching. This broad specificity for branching may also explain why A59-PS(S_p) and U80-PS(S_p) spliceosomes also catalysed exon ligation in the presence of thiophilic metals, whereas G60-PS(R_p), G78-PS(S_p), and U80-PS(R_p) spliceosomes, for which branching was only rescued in the presence of Cd^{2+} , stalled after branching. Values are averages; error bars, s.d. ($n = 3$).



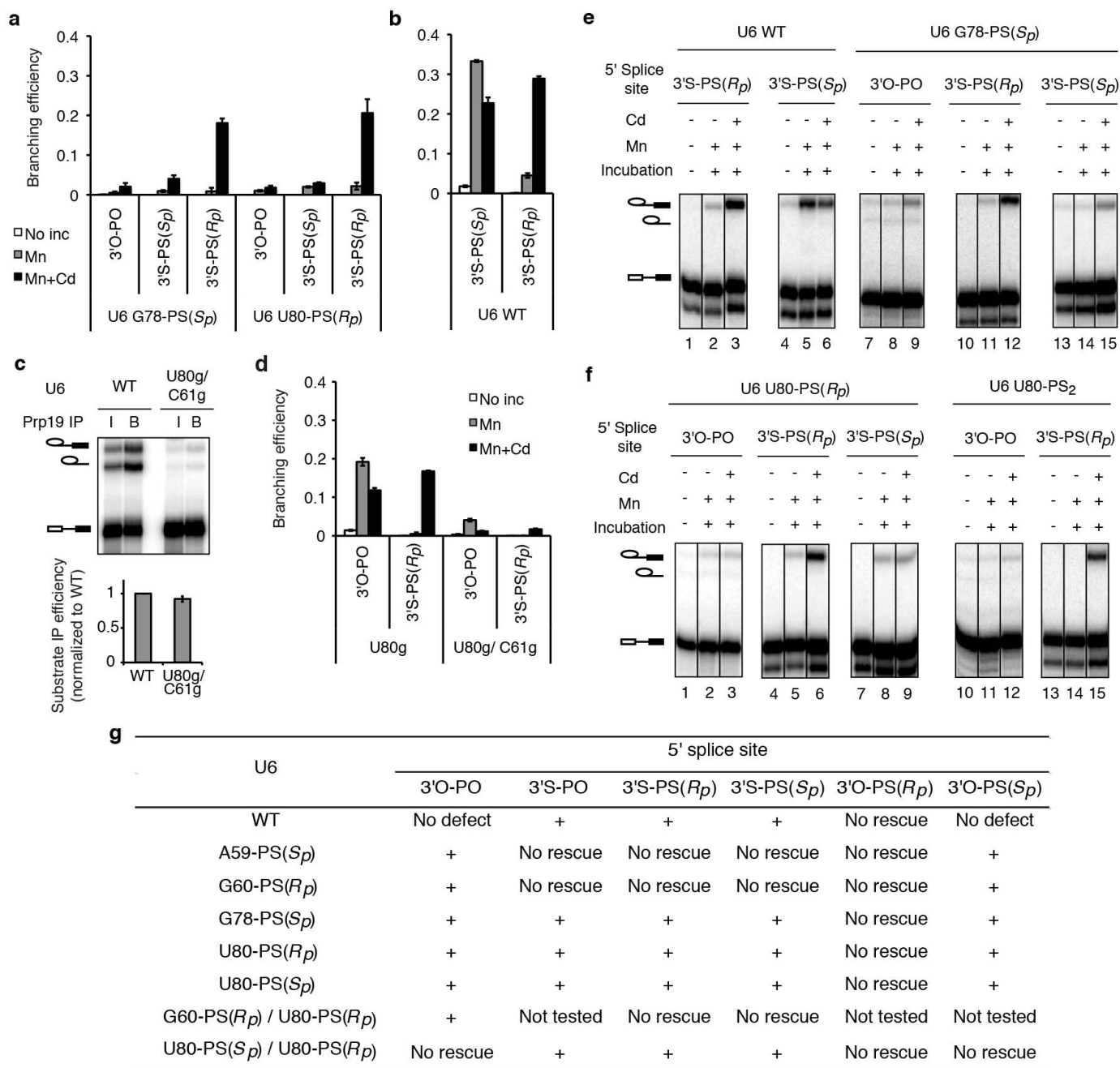
Extended Data Figure 3 | A divalent metal binds the 5' splice site *pro-R_p* oxygen during branching. **a**, *UBC4* pre-mRNAs bearing the indicated modifications at the 5' splice site (top panel) were assayed as in Fig. 3a. The band marked * results from 5' to 3' exonucleolytic degradation that is blocked by the sulphur; ** denotes statistical significance of Cd²⁺ rescue compared to Mg²⁺ splicing ($P = 0.004$, paired, one-tailed *t*-test, $n = 3$). The data from Fig. 3a are reproduced here to aid comparison. Values are averages; error bars, s.d. ($n = 3$); no inc, no incubation. **b**, Mapping of the site of branching. Purified, ³²P-labelled, intact lariat intermediates (LI ~ 0.2 fmol) resulting from branching of the *UBC4* 3'O-PO or 3'S-PS(*R_p*) substrates were used as templates for reverse transcriptase (RT) using primer IP3 (~10 fmol), which

binds at nucleotides +5 to +24 of the intron (see lower diagram). Lanes 6 and 7 show that the major RT stop occurs at the same position when either the 3'O-PO or 3'S-PS(*R_p*) lariats are used as template. This stop migrates at the expected position, which is the position of the ddC stop resulting from extension of primer IP3 with pre-mRNA as template and therefore corresponds to position +1 of the intron, the expected branch site. Lower diagram shows mapping of the primer and expected RT stop onto the *UBC4* pre-mRNA sequence; bold exon; italics intron. Note that the band marked *** is present in the ³²P pre-mRNA lane and thus is probably a nonspecific band resulting from contamination with pre-mRNA degradation products that can anneal to the primer and serve as template.



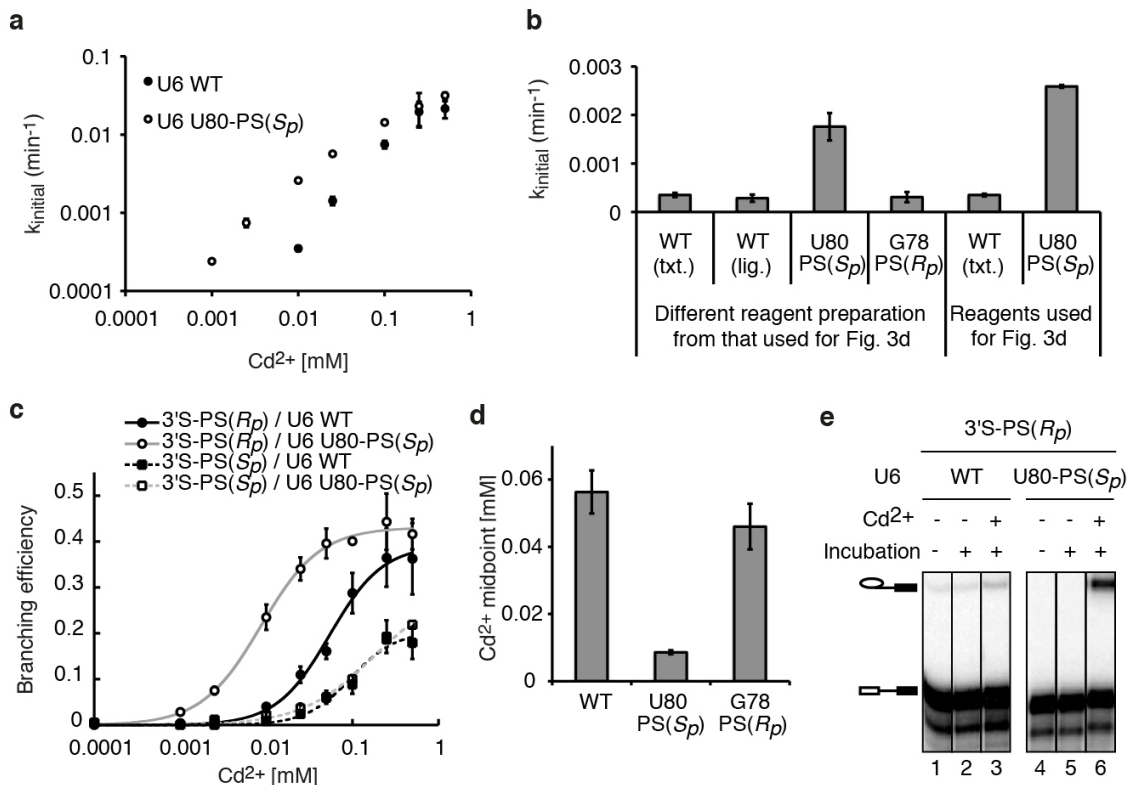
Extended Data Figure 4 | The *UBC4* 3'S substrate can be branched efficiently only in the presence of thiophilic metals. **a**, A sulphur at the 5' splice site leaving group alone blocked splicing in extract. Following affinity-purification branching efficiency was quantified (bottom) without further incubation. Note that immunoprecipitation of pre-mRNA indicated that the sulphur did not block the catalytic activation of the spliceosome. **b**, Thiophilic metals rescued the branching defect of the 3'S substrate. Spliceosomes were assayed in buffer PK (pH 7.0) in the presence of 2 mM total metal (1 mM MgCl_2 plus 1 mM MnCl_2 or 1 mM CdCl_2) for 1.5 h. The bar graph quantifies the relative stimulation by specific metals (normalized to Mg^{2+}). **c**, **d**, Thiophilic

metals specifically stimulate branching of the 3'S, but not the 3'O substrate. Affinity-purified spliceosomes from extracts depleted of Cwc25p, to stall spliceosomes independent of the sulphur substitution, were incubated as in Fig. 3a except that washes and incubation were done in buffer DK without EDTA and with 1 mM MgCl_2 ; rCwc25 as well as an HP extract fraction were also added to complement (Supplementary Note 4; Methods). Quantification of the thiophilic metal stimulation relative to Mg^{2+} is shown both for reaction endpoints (c) and for the rate of branching (d). Values are averages; error bars, s.d. ($n = 3$). The band marked * results from 5' to 3' exonucleolytic degradation that is blocked by the sulphur.



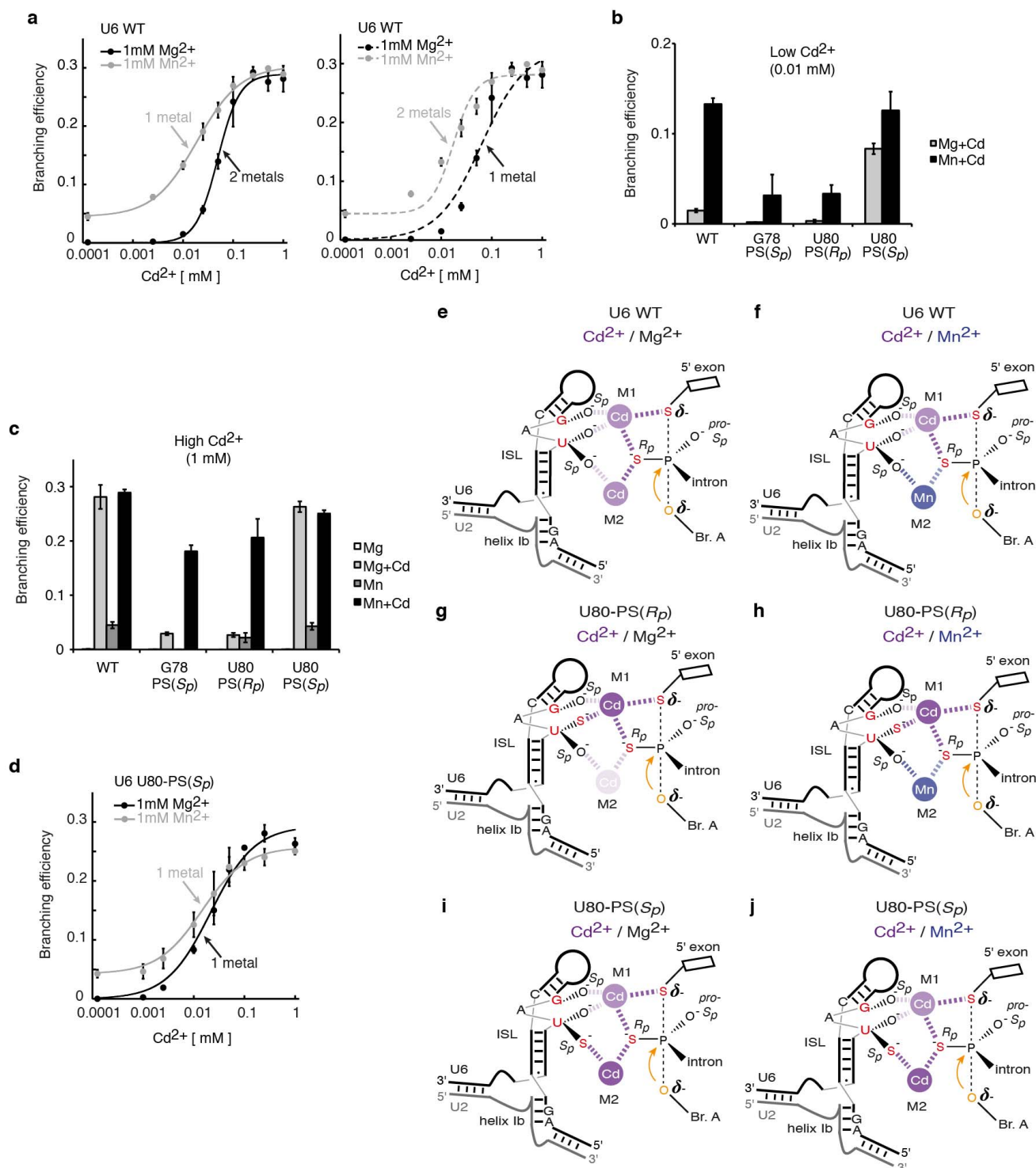
Extended Data Figure 5 | The 3'S-PS(*R_p*) substrate specifically improves rescue for spliceosomes containing U6 sulphur substitutions that compromise catalytic metal binding. **a, b**, Spliceosomes were assayed as in Fig. 3b. Note that the 3'S-PS(*S_p*) substrate does not significantly improve Cd²⁺ rescue when compared to the 3'O-PO substrate (**a**), despite having similar reactivity to the 3'S-PS(*R_p*) substrate with wild-type U6 (**b**). **c**, The U6 double mutation U80g/C61g permitted both spliceosome assembly and activation, as reflected by the stable association of Prp19p with the splicing substrate. 10% of the RNA in the input (I) for the immunoprecipitation or 100% of the RNA associated with affinity-purified spliceosomes (B) were analysed by denaturing PAGE (top). Total immunoprecipitation efficiency was quantitated for all

splicing species combined (bottom). **d**, The 3'S-PS(*R_p*) substrate did not significantly improve splicing for U80g and U80g/C61g spliceosomes. Assays were as in Fig. 3b. **e, f**, Representative raw data for Fig. 3. Assays were as in Fig. 3. In **e**, for wild-type U6 lanes 1–3 and 4–6 were taken from two different gels, for G78-PS(*S_p*) lanes 7–12 and 13–15 were taken from two different gels. In all other cases the lanes for different substrates assembled with spliceosomes bearing the same U6 modification were taken from the same gel. Values are averages; error bars, s.d. (*n* = 3 for **a, b, d**; *n* = 2 for **c**); no inc., no incubation. **g**, Summary of combinations of sulphur substitutions in U6 and the substrate tested for rescue of branching. The + sign indicates that branching was observed in the presence of thiophilic metal.



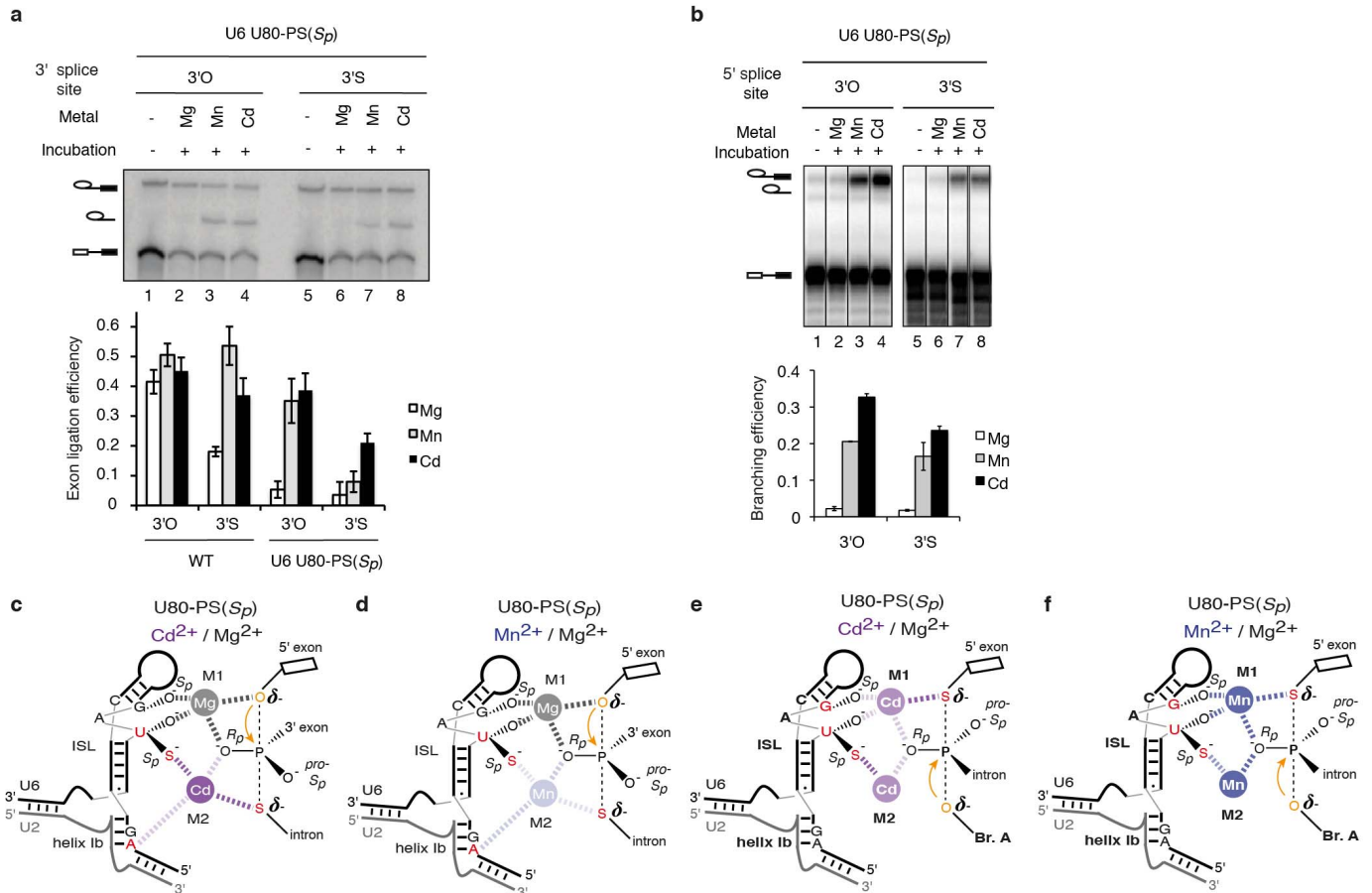
Extended Data Figure 6 | U6 snRNA positions catalytic metals during branching: controls for the U80-PS(S_p) induced shift in the Cd^{2+} transition midpoint for rescue of the 3'S-PS(R_p) substrate. **a**, The shift induced by U80-PS(S_p) in the Cd^{2+} midpoint for rescue was also observed when reaction rates, instead of amplitudes, were compared. Initial rates are plotted versus CdCl_2 concentration. Assays were as in Fig. 3d. Values are averages; error bars represent s.d. ($n = 2$). Initial rates, rather than apparent overall rates, were used here because the branching efficiency did not level off by 120 min at Cd^{2+} concentrations below 0.025 mM (assuming an endpoint of ~ 0.4). In support of this approach, at saturating Cd^{2+} both wild-type and U80-PS(S_p) spliceosomes branched similar fractions of the 3'S-PS(R_p) substrate (see **c**), indicating that addition of a sulphur in U6 within the catalytic core did not necessarily alter the population of complexes that are competent for catalysis. **b**, Transcribed (txt.) and ligated (lig.) wild-type U6 behaved similarly relative to U80-PS(S_p) for branching of the 3'S-PS(R_p) substrate at a limiting Cd^{2+} concentration. Initial rates are shown for branching of the 3'S-PS(R_p) substrate in the presence of 0.01 mM Cd^{2+} . **c**, A sulphur at U80 *pro-S_p* shifts the Cd^{2+} titration midpoint

for rescue of the 3'S-PS(R_p) substrate relative to the 3'S-PS(S_p) substrate. Assays were as in Fig. 3d; the 3'S-PS(R_p) data from Fig. 3d are shown again here for comparison. Curves represent Hill fits to the data. Values are averages; error bars, s.d. ($n = 3$). Although the Cd^{2+} titration for rescue of U80-PS(S_p) spliceosomes assembled on the 3'S-PS(S_p) substrate did not plateau under our experimental conditions (panel **c**), the data nevertheless set a lower limit for the apparent transition midpoint; further, this midpoint is equal to or greater than that observed for U6 wild-type spliceosomes, indicating that the shift by U80-PS(S_p) of the Cd^{2+} transition midpoint for rescue was specific for the 3'S-PS(R_p) substrate. **d**, With the 3'S-PS(R_p) substrate, U80-PS(S_p) decreased the Cd^{2+} titration midpoint for rescue of branching by sixfold. The apparent midpoint for G78-PS(R_p) spliceosomes is shown as an additional specificity control for the shift observed for U80-PS(S_p) (actual titration data not shown). The apparent Cd^{2+} rescue midpoints were obtained by fitting titration curves to the general Hill equation (see Methods). Error bars represent error of the Hill fit. **e**, Representative raw data for Fig. 3d. Assays were in the presence of 0.01 mM Cd^{2+} when indicated.



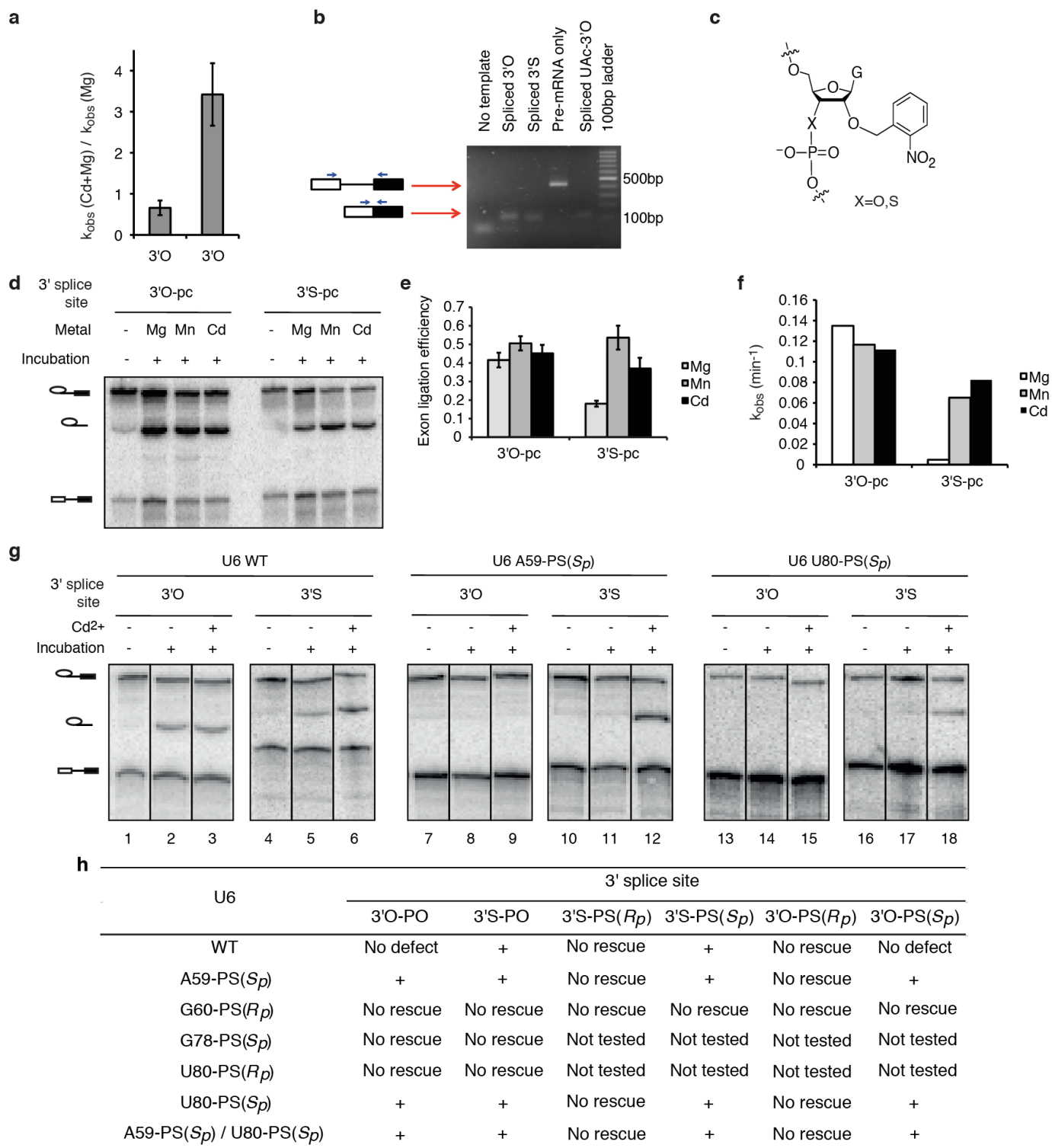
Extended Data Figure 7 | Further evidence for two distinct catalytic metal sites during branching. **a**, Branching requires two catalytic divalent metals. **b–d**, The 5' splice site *pro-R_p* oxygen and the U80 *pro-S_p* oxygen interact with a metal distinct from the metal that interacts with the 5' splice site *pro-R_p* oxygen and the U80 *pro-R_p* and G78 *pro-S_p* oxygens. See Supplementary Note 7 for discussion. Spliceosomes were assayed for branching as in Fig. 3e; where indicated, $MgCl_2$ or $MnCl_2$ were present at 1 mM. Curves represent Hill fits to the data. The data in **a** are reproduced here from Fig. 3e to aid comparison. In panels **a–d**, values are averages; error bars, s.d. ($n = 3$). Cd^{2+} was limiting in **b** to sensitize the assay to binding of a second metal, and Cd^{2+} was saturating in **c** to show that G78-PS(S_p) and U80-PS(S_p) have the potential to be rescued at levels comparable to wild-type U6. Panel **d** shows that U80-PS(S_p) eliminates

the affect of Mn^{2+} on the titration curves. **e–j**, Metal binding during branching for different combinations of sulphur substitutions in the substrate and U6 in the presence of the indicated metals, as reflected by the data in panels **a–d**. Panels **e** and **f** reflect data in **a**, **b** and **c**; panels **g** and **h** reflect data in **b** and **c**; panels **i** and **j** reflect data in **b**, **c** and **d**. Relevant U6 ligands are coloured red in each panel; the nucleophile is coloured orange. Metals are coloured magenta (Cd^{2+}) and blue (Mn^{2+}), and their interactions with specific U6 ligands are depicted as dashed lines, with differential shading intensity meant to illustrate differences in the expected strength of interaction with oxygen compared with sulphur, as inferred from studies with model compounds^{38,61}. Shading of metals bound at M1 and M2 is further adjusted to reflect experimental observations. Panels for G78-PS(S_p) would look the same as those for U80-PS(R_p) (**g** and **h**).



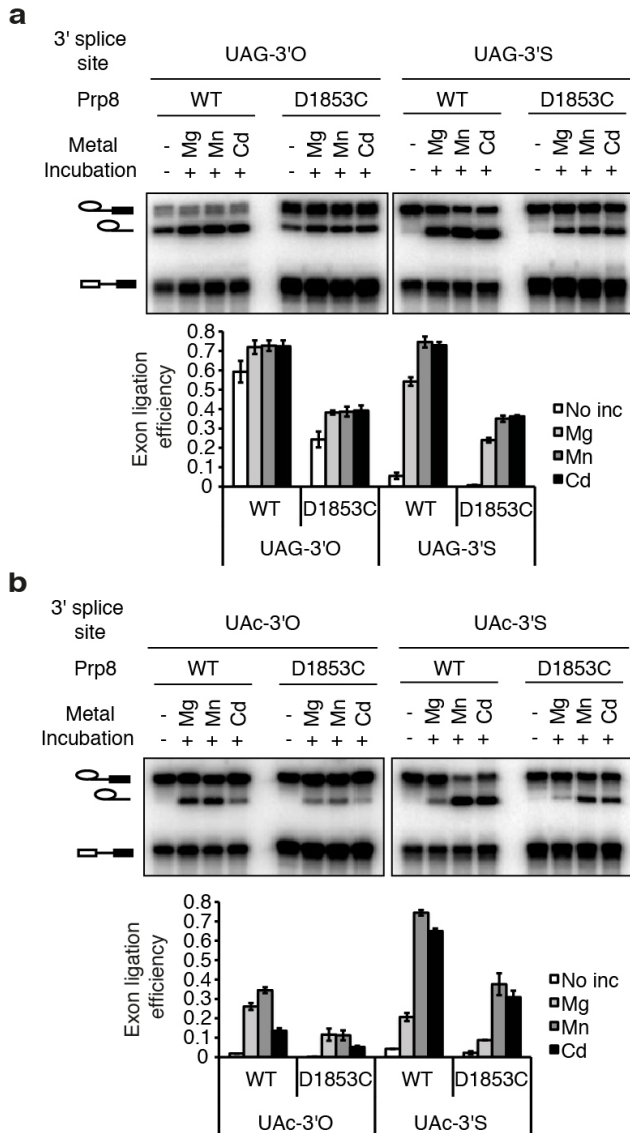
Extended Data Figure 8 | A sulphur at the 3' splice site but not the 5' splice site leaving group alters the metal specificity for rescue of U80-PS(*S_p*) spliceosomes: further evidence that U80 interacts with a catalytic metal during exon ligation. **a**, A sulphur at the 3' splice site leaving group during exon ligation alters the metal specificity for rescue of U80-PS(*S_p*) spliceosomes. Assays were as in Fig. 2j. The bar graph depicts quantification of exon ligation efficiency. **b**, A sulphur at the 5' splice site leaving group during branching does not alter the metal specificity for rescue of U80-PS(*S_p*)

spliceosomes. Assays were as in Fig. 3a, except with the 3'S-PO substrate. Values are averages; error bars, s.d. ($n = 3$). **c-f**, Inferred metal binding during exon ligation (**c**, **d**) and branching (**e**, **f**) for the indicated combinations of sulphur substitutions in the substrate and U6 in the presence of the indicated metals. Relevant U6 ligands are coloured red in each panel; the nucleophile is coloured orange. Metals and ligand interactions are coloured as in Extended Data Fig. 7.



Extended Data Figure 9 | Thiophilic metals rescue exon ligation for substrates containing a sulphur at the 3' splice site leaving group in both a mutated and wild-type 3' splice site context. **a**, Cd²⁺ specifically stimulates the rate of exon ligation for the mutated, UAc-3'S substrate. Assays were as in Fig. 4a. **b**, Exon ligation occurs at the correct site for the 3'S substrate. RNA from affinity-purified spliceosomes assembled on ACT1-3'O, ACT1-3'S, and ACT1-UAc-3'O and chased as in Fig. 4a was subjected to RT-PCR using the primers depicted in blue arrows. **c**, Diagram of the photocaged linkage at the 3' splice site. **d-f**, Cd²⁺ specifically stimulates the rate of exon ligation for the

wild-type, UAG-3'S substrate. Assays were as in Fig. 4a, except that before addition of divalent metals, samples were irradiated with 308 nm light on ice for 5 min to remove the photocage. Shown are a representative gel (**d**), quantification of the reaction end points (**e**) and quantification of reaction rates (**f**). **g**, Representative raw data for Fig. 4b; bands within each set came from non-adjacent lanes on the same gel. Values are averages; error bars, s.d. ($n = 3$). **h**, Summary of combinations of sulphur substitutions in U6 and the substrate tested for rescue of exon ligation. The + sign indicates that exon ligation was observed in the presence of thiophilic metal.



Extended Data Figure 10 | Residue D1853 of the RNaseH-like domain of Prp8 does not have a direct role in metal-mediated catalysis of exon ligation. **a, b,** Spliceosomes assembled on the indicated ACT1 UAG (**a**) or UAc (**b**) 3'O or 3'S substrates were assayed as in Fig. 2j, in the absence of ATP. Splicing extracts were prepared from either a wild-type *PRP8* strain or a mutant strain having the *prp8-D1853C* mutation. See Supplementary Note 15 for details and a discussion. Values are averages; error bars, s.d. ($n = 2$); no inc, no incubation.